Summer 2017

Study on the dispersion of particles at a fluid-liquid interface and its application in hydrophilous pollination

Naga Aditya Musunuri
New Jersey Institute of Technology

Copyright Warning & Restrictions

The copyright law of the United States (Title 17, United States Code) governs the making of photocopies or other reproductions of copyrighted material.

Under certain conditions specified in the law, libraries and archives are authorized to furnish a photocopy or other reproduction. One of these specified conditions is that the photocopy or reproduction is not to be "used for any purpose other than private study, scholarship, or research." If a, user makes a request for, or later uses, a photocopy or reproduction for purposes in excess of "fair use" that user may be liable for copyright infringement,

This institution reserves the right to refuse to accept a copying order if, in its judgment, fulfillment of the order would involve violation of copyright law.

Please Note: The author retains the copyright while the New Jersey Institute of Technology reserves the right to distribute this thesis or dissertation

Printing note: If you do not wish to print this page, then select "Pages from: first page # to: last page #" on the print dialog screen

ABSTRACT

STUDY ON THE DISPERSION OF PARTICLES AT A FLUID-LIQUID INTERFACE AND ITS APPLICATION IN HYDROPHILOUS POLLINATION

by
Naga Aditya Musunuri

This dissertation work describes the physics of particle adsorption and the spontaneous dispersion of powders that occurs when they come in contact with a fluid-liquid interface and its application in hydrophilous pollination of Ruppia Maritima, an aquatic plant. The dispersion of particles can occur so quickly that it appears explosive, especially for small particles on the surface of mobile liquids like water. PIV (Particle Image Velocimetry) measurements show that the adsorption of a spherical particle at the interface causes an axisymmetric streaming flow about the vertical line passing through the particle center. The fluid directly below the particle rises upward, and near the surface, it moves away from the particle. The flow, which develops within a fraction of a second after the adsorption of the particle, persists for several seconds. The flow strength, and the volume over which it extends, decrease with decreasing particle size. The streaming flow induced by the adsorption of two or more particles is a combination of the flows which they induce individually. The flow causes particles sprinkled together onto a liquid surface to disperse, as well as to hydrodynamic stresses which is extensional in the plane tangential to the interface and compressive in the normal direction. The stresses can cause the breakup of particle agglomerates when they are adsorbed on a liquid surface.

The physics underlying the mechanisms of two-dimensional aquatic pollen dispersal, known as hydrophily is also studied and presented here. The aquatic pollination has evolved in several genera of aquatic plants, including *Halodule*,

Halophila, *Lepilaena*, and *Ruppia*. *Ruppia maritima*, which is native to salt and brackish waters circumglobally, is selected for this study. Two mechanisms are observed, by which the pollen released from male inflorescences of *Ruppia* is adsorbed on a water surface: 1) inflorescences rise above the water surface and after they mature their pollen mass falls onto the surface as clumps and disperses as it comes in contact with the surface; 2) inflorescences remain below the surface and produce air bubbles which carry pollen mass to the surface where it disperses. In both cases dispersed pollen masses combined with others under the action of lateral capillary forces to form pollen rafts. The formation of porous pollen rafts increases the probability of pollination since the attractive capillary force on a pollen raft toward a stigma is much larger than on a single pollen grain. The presence of a trace amount of surfactant can disrupt the pollination process as the pollen is not captured or transported on the water surface.

STUDY ON THE DISPERSION OF PARTICLES AT A FLUID-LIQUID INTERFACE AND ITS APPLICATION IN HYDROPHILOUS POLLINATION

by
Naga Aditya Musunuri

A Dissertation
Submitted to the Faculty of
New Jersey Institute of Technology
in Partial Fulfillment of the Requirements for the Degree of
Doctor of Philosophy in Mechanical Engineering

Department of Mechanical and Industrial Engineering

August 2017

.

APPROVAL PAGE

STUDY ON THE DISPERSION OF PARTICLES AT A FLUID-LIQUID INTERFACE AND ITS APPLICATION IN HYDROPHILOUS POLLINATION

Naga Aditya Musunuri

Dr. Pushpendra Singh, Dissertation Advisor — Date
Professor of Mechanical and Industrial Engineering, NJIT

Dr. Ian S. Fischer, Co-Advisor — Date
Professor of Mechanical and Industrial Engineering, NJIT

Dr. Daniel E. Bunker, Co-Advisor — Date
Associate Professor of Federated Department of Biological Sciences, NJIT

Dr. Siva P.V. Nadimpalli, Committee Member — Date
Assistant Professor of Mechanical and Industrial Engineering, NJIT

Dr. I. Joga Rao, Committee Member — Date
Chair and Professor of Mechanical and Industrial Engineering, NJIT

Dr. Anthony D. Rosato, Committee Member — Date
Professor of Mechanical and Industrial Engineering, NJIT

Dr. Shawn A. Chester, Committee Member — Date
Professor of Mechanical and Industrial Engineering, NJIT

BIOGRAPHICAL SKETCH

Author: Naga Aditya Musunuri

Degree: Doctor of Philosophy

Date: August 2017

Undergraduate and Graduate Education:

- Doctor of Philosophy in Mechanical Engineering,
  New Jersey Institute of Technology, Newark, NJ, 2017

- Master of Science in Mechanical Engineering,
  New Jersey Institute of Technology, Newark, NJ, 2011

- Bachelor of Science in Mechanical Engineering,
  Jawaharlal Nehru Technological University, Hyderabad, India, 2009

Major: Mechanical Engineering

Presentations and Publications:

N. Musunuri, D. Bunker, S. Pell, I. Fischer and P. Singh, Fluid Dynamics of Hydrophilous Pollination in Ruppia (widgeon grass), *Procedia IUTAM*(2017).

N. Musunuri, D. Bunker, S. Pell, I. Fischer an P. Singh, Fluid Dynamics of Two-Dimensional Pollination in Ruppia (widgeon grass), ASME Paper Number FEDSM2016-7891, New York: American Society of Mechanical Engineers, Washington D.C (2016).

E. Amah, Md. Hossain, N. Musunuri, I. Fischer and P. Singh, Electric Field Driven Hierarchical Self-assembly of Monolayers of Mixtures of Particles, 24th International Congress of Theoretical and Applied Mechanics (ICTAM 2016) pp.1168-1169, Montreal, Canada, August 2016.

N. Musunuri, K. Shah, H. Hossain, S. Gurupatham, E. Amah, I.S. Fischer, and P. Singh, Electric Field Driven Hierarchical Self-assembly of Monolayers of Mixtures of Particles, Annual Transactions of the Nordic Rheology Society, vol. 23, 2015, Karlstad, Sweden, August 19-20 (2015).

P. Singh, N. Musunuri and I. Fischer, Spontaneous Dispersion of Particles on Fluid-liquid Interfaces, Annual Transactions of the Nordic Rheology Society, vol. 23, 2015, Karlstad, Sweden, August 19-20 (2015).

N. Musunuri, B. Dalal, D. Codjoe, I. Fischer and P. Singh, Transient Flow Induced by the Adsorption of Particles, KONA Powder and Particle Journal no.31 (2014) 135-145.

N. Musunuri, P. Singh and I. Fischer, PIV Measurements of the Transient Fluid Flow Due to the Adsorption of Particles, 4th Joint US-European Fluids Engineering Division Summer Meeting (FEDSM 2014), Chicago, IL, August 2014.

S. Pillapakkam, P. Singh and N. Musunuri, Self-Assembly of Monolayers of Submicron Sized Particles on Thin Liquid Films, ASME Paper Number IMECE2013-65324, New York: American Society of Mechanical Engineers, San Diego, CA (2013).

N. Musunuri, B. Dalal, D. Codjoe, I. Fischer and P. Singh, Transient Flow Induced by the Adsorption of Particles, ASME Fluids Engineering Division Summer Meeting (FEDSM 2013), Incline Village, NV, July 2013.

M. Hossain, K. Shah, D. Jhu, S. Gurupatham, I.S. Fischer, N. Musunuri and P. Singh, Self-assembly of monolayers of micron sized particles on thin liquid films, ASME Paper Number FEDSM2013-16271, New York: American Society of Mechanical Engineers, Incline Village, NV, July 2013.

P. Singh, I. Fischer, B. Dalal, S. Gurupatham, Md. Hossain and N. Musunuri, Dispersion of particles on Fluid-Liquid Interfaces, 23rd International Congress of Theoretical and Applied Mechanics (ICTAM 2012), Beijing, China, August 2012.

ACKNOWLEDGMENT

It is only fair to begin by acknowledging the unending support and encouragement from my parents and my sister throughout my life.

My sincere thanks and gratitude to my co-advisor Dr. Pushpendra Singh, for his belief in me and for his continuous trust and guidance, he bestowed upon me right from day 01. He has been advising me through the highs and lows of my performance and I believe he will continue to do so for the rest of my career. My co-advisors Dr. Ian Fischer from Mechanical Engineering Department and Dr. Daniel Bunker from the Federated Department of Biological Sciences, have been great mentors at crucial junctures of my research life. I would also like to extend my thanks to all the committee members, especially to Dr. Joga Rao, who encouraged me right from when I was a master's student. Thank you, all the professors/lecturers, who taught me during my masters and doctoral student life and all the professors/lecturers with whom I worked with as a teaching assistant.

Thank you to all the MIE departmental administrative staff including Joseph Glaz and his crew (Gregory Policastro and Nicholas Muscara), Yvonne Williams, Barbara Valenti and Aileen Checa for all the help they provided.

I would like to acknowledge the support of my friends and fellow graduate and undergraduate students in our research group. This section would be incomplete, without the mention of my extended family in New Jersey consisting of my cousins and their families. They have always been there to support me all through my life in the USA.

Dedicated to my parents Mr. Sri Krishna Sudarsana Anandam Musunuri and Mrs. Vijaya Lakshmi Musunuri, and my sister Udaya Musunuri.

TABLE OF CONTENTS

TABLE OF CONTENTS
(Continued)

LIST OF FIGURES

List of Figures
(Continued)

List of Figures
(Continued)

CHAPTER 1

INTRODUCTION

1.1 Objective

The objective of this dissertation is to understand the physics behind the adsorption of particles at a fluid-liquid interface, measure the transient flow created due to adsorption and study the application of this phenomenon in hydrophilous pollination (pollination on water surface) of Ruppia Maritima, a water plant.

1.2 Background Information on Adsorption of particles at Fluid-Liquid Interfaces

Past studies have been concerned with understanding the mechanisms by which particles already trapped on fluid-liquid interfaces interact leading to their self-assembly into monolayered patterns[1-3], the sudden dispersion of particles coming into contact with a fluid-liquid interface described in this work has not been considered prior to our recent study [4-6].

It was shown in [6] that (i) particles sprinkled over a small area almost instantaneously spread over an area that can be several orders of magnitudes larger (see Figure 1.1); (ii) a newly-adsorbed particle causes particles already trapped on the interface to move away creating a particle-free region around itself (see Figure 1.2); and (iii) dispersion influences the nature, e.g., structure and porosity, of the monolayer clusters that are formed. These phenomena have importance in a wide range of applications, such as pollination in hydrophilous plants, transportation and spreading of

microbes and viruses, and the self-assembly of particles leading to the formation of novel nano-structured materials, stabilization of emulsions, etc. [7-15]

The dispersion can occur so quickly that it appears *explosive*, especially on the surface of mobile liquids like water. An experiment showing this can be performed easily in a household kitchen by filling a dish partially with water and then sprinkling a small amount of a finely-ground powder such as wheat or corn flour onto the water surface. The moment the flour comes in contact with the surface it quickly disperses into an approximately-circular shaped region, forming a monolayer of dispersed flour particles on the surface (see Figure 1.1). The interfacial forces that cause this sudden dispersion of flour particles are, in fact, so strong that a few milligrams of flour sprinkled onto the surface almost instantaneously covers the entire water surface in the dish.

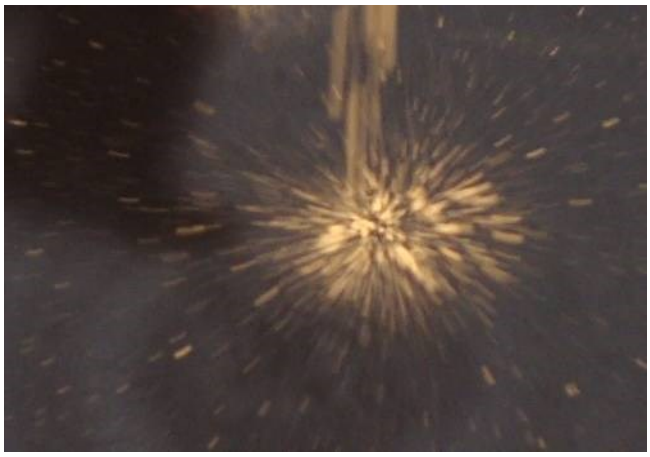

Figure 1.1 Sudden dispersion of flour sprinkled onto water in a dish. Streaklines were formed due to the radially-outward motion of the particles emanating from the location where they were sprinkled. The size of flour particles was ~2-100 μm.

Source: [5]

It was shown by [4, 6] that the initial dispersion of particles is due to the fact that when a particle comes in contact with the interface, the vertical capillary force pulls it into the interface, thereby causing it to accelerate in the direction normal to the interface

(see Figure 1.2). The maximum velocity increases with decreasing particle size; for nanometer-sized particles, e.g., viruses and proteins, the velocity on an air-water interface can be as large as ~47 m/s. Also, since the motion of a particle on the surface of mobile liquids like water is inertia dominated, it oscillates vertically about its equilibrium height before the viscous drag causes it to stop. This gives rise to a *streaming* flow on the interface away from the particle (see Figure 1.2c).

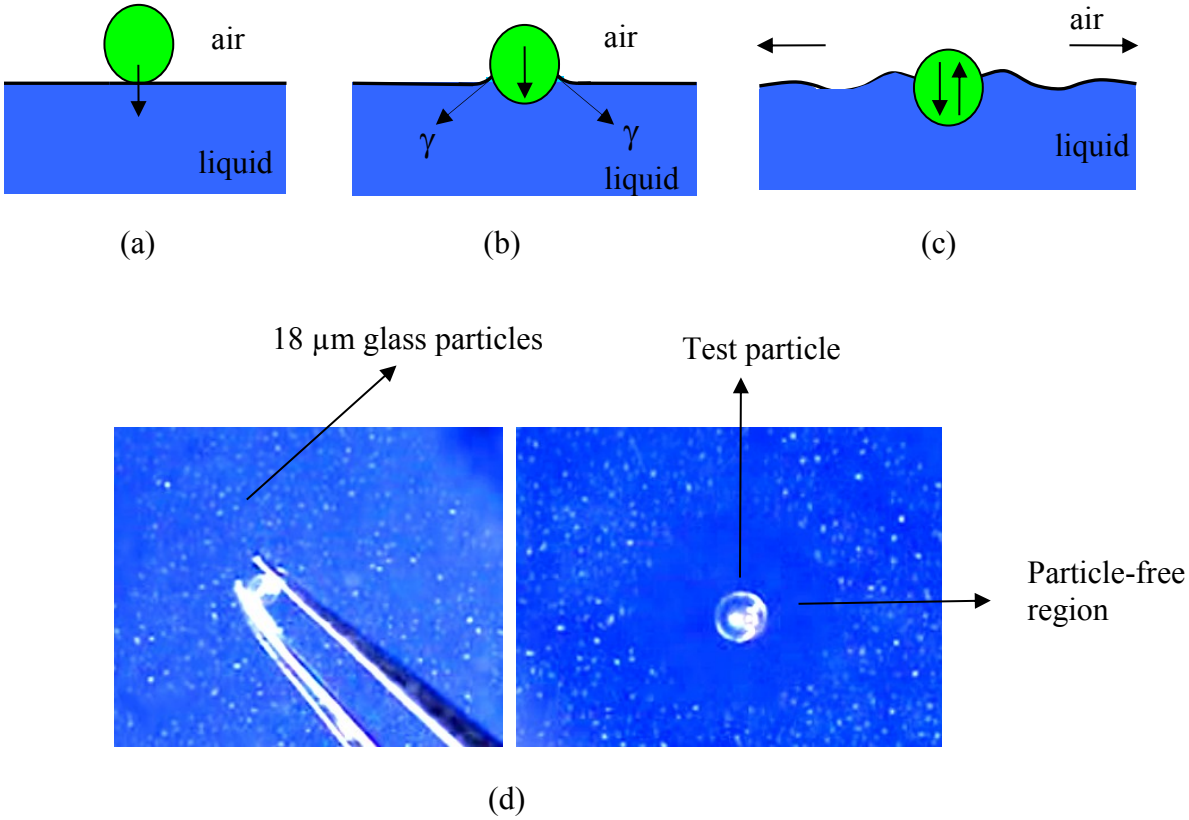

Figure 1.2 Trapping (or adsorption) of particles at an interface. (a) The particle comes in contact with the interface. (b) The particle is pulled downwards by the interfacial force (γ_{12}). (c) The particle oscillates about the equilibrium height within the interface causing a radially outward flow on the interface. (d) (Left) A glass sphere of diameter 1.1 mm being dropped onto a monolayer of 18 µm tracer glass particles on the surface of 60% glycerin in water. (Right) The flow on the surface causes all of the nearby tracer particles to move away so that a roughly circular, particle-free region is created.

The energy needed to pull a particle into the interface and to induce the streaming flow comes from the net *decrease* in the interfacial energy (W_a) due to the adsorption of the particle [6]. By assuming that the particle floats without significantly deforming the interface, it can be shown that W_a for a spherical particle of radius *R* is

$$W_a = \pi R^2 \gamma_{12}(1+\cos\theta)^2 \tag{1.1}$$

where θ is the contact angle and γ_{12} is the interfacial tension between the upper and lower fluids [8, 16].

Therefore, when two or more particles are simultaneously adsorbed at the interface, each of the particles causes a streaming flow on the interface away from itself thereby causing the other particles to move away. When two particles are adsorbed the maximum distance by which they move apart is about a few diameters. But, as the number of particles being adsorbed increases, the distance travelled by a particle, especially if it is near the outer periphery of the cluster, can be very large—several orders of magnitude larger than any dimension of the area over which particles are sprinkled. For example, as noted above, a few milligrams of flour sprinkled over a very small area on the water surface almost spontaneously disperses to cover the entire water surface in the dish.

The dispersion phase, which lasts for a short period of time (about one second for the case described in Figure 1.1), is followed by a phase that is dominated by attractive lateral-capillary forces during which particles slowly come back to cluster. The latter phase has been a focus of many past studies [1, 2, 17, 18]. Particles trapped at a fluid-fluid interface generally interact with each other via attractive capillary forces that arise

because of their weight. A common example of this capillarity-driven self-assembly is the clustering of breakfast-cereal flakes floating on the surface of milk. This mechanism is widely used for two-dimensional assembly of particles at liquid surfaces. However, if the buoyant weight of particles is negligible, as is the case for colloidal particles, then the particles will only disperse since the attractive capillary forces between them are negligible [19-22].

One may postulate that the gradient of particle concentration gives rise to a (Marangoni) force that causes particles to disperse because the concentration of particles in the region in which they are sprinkled is larger than in the surrounding region. However, this is clearly not the case, as the dispersed particles cluster again under the action of lateral capillary forces. This shows that the gradient of particle concentration does not give rise to a dispersion force and that particles disperse only when they come in contact with the interface for the first time (during which each of the particles gives rise to a flow away from itself as they are pulled into the interface).

Also, one may postulate that the dispersion is because of the presence of contaminants on the surface of particles which are released into the liquid when they come in contact with the interface and their presence in fact causes particles to disperse. If this is the case, then the intensity with which the particles disperse should diminish when they are washed. We ruled out this possibility by repeatedly washing the particles and showing that their dispersive behavior did not change when the experiments were repeated [4].

Particles also disperse on liquid-liquid interfaces. In fact, as Figure 1.3 shows, the dispersion forces can break apart agglomerates of micron-sized particle that remain intact

in the upper liquid [5]. This breakup and spreading of particle clumps (agglomerates) on liquid surfaces is important in various processes in the pharmaceutical and food industries such as wet granulation and food processing [23-25]

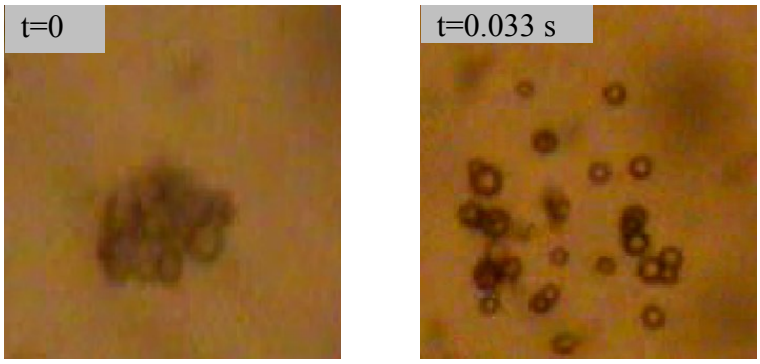

Figure 1.3 Breakup and dispersion of an agglomerate on the interface of corn oil and water, looking down from above (500x mag.). The size of glass particles of the agglomerate was ~4 μm. (left) An agglomerate sedimented through corn oil and was captured at the interface. (right) After coming in contact with the interface it *breaks apart explosively* dispersing radially-outward into an approximately-circular region. Notice that some of the particles remained agglomerated.

Source: [5]

The sudden dispersion of particles plays an important role also in some physical processes occurring on fluid-fluid interfaces, including the rate at which germs/microbes disperse on a water surface. An example in botany is the formation by hydrophilous (water-pollinated) plants of floating porous pollen structures called “pollen rafts” [9, 10]. A crucial first step in their formation is the initial dispersion of pollen that occurs after it comes in contact with the water surface (if it did not disperse, it would remain clumped/agglomerated).

1.3 Literature Review

The behavior of particles trapped at gas-liquid interfaces has come under intense scrutiny in recent years because of their importance in a wide range of applications, such as in waste-water treatments [70], mineral and solvent extractions processes [14], adsorption of colloidal particles onto an air-water interface for generating films [77], preparation of anti-stick surfaces [78], separation of ink and toner particles [15], self-assembly of particles at fluid–fluid interfaces [4-10], stabilization of emulsions[7], pollination in hydrophilous plants [9], flotation of insect eggs [10,21,79], dispersion of viruses and protein macromolecules [79], pharmaceutical [18-21] and food industries [41].

The mechanics by which particles are captured and move on fluid-liquid surfaces (either gas-liquid or liquid-liquid interfaces), and their subsequent interactions leading to self-assembly of monolayer patterns is very interesting. Particles captured on a liquid surface may be colloidal or non-colloidal. When a particle comes in contact with a fluid-liquid interface it is pulled inwards to its equilibrium position within the interface by the vertical component of the capillary and gravity forces [23]. The equilibrium position of an adsorbed particle in the interface is determined by the balance of the particle's buoyant weight, the vertical capillary force and any other force (with a vertical component) that acts on the particle. The particle is in stable equilibrium in the sense that if it is moved away from its equilibrium position, a restoring capillary force acts to bring it back. However, if the capillary force is not sufficiently large to overcome the buoyant weight, a balance of the forces in the direction normal to the interface is not possible and the particle is not trapped in the interface. This is normally the case for millimeter and larger-sized particles that are heavier than the liquid below. Micron and nano-sized particles, on

the other hand, for which the buoyant weight is negligible compared to the capillary force, are readily trapped at the interface

Though small particles first dispersed violently at large speeds, later they slowly came back to form monolayer clusters due to attractive lateral capillary forces. The same dynamics were observed for more viscous liquids except that the dispersion speeds were smaller. The fluid dynamics of the attractive phase are well understood [8-16], but surprisingly there is no mention in the past studies of the initial violent dispersion of particles despite the fact that this dispersion is ubiquitous, and occurs for many common liquids and particles.

Though the particle dispersion is ubiquitous it has remained a mystery over many decades. But, this phenomenon has been the root cause of formation of a porous pollen structure known as “pollen rafts” in which an important first step is the initial dispersion of pollen occurring after it comes in contact with the water surface [9]. Authors [9] did not give a reason for the initial dispersion of pollen.

After this initial dispersion, the pollen particles (usually, form a single anther) cluster to form a pollen raft. It was shown in references [9] and [10] that the formation of porous pollen rafts increases the probability of pollination, because the surface area of the raft is much greater than that of a single pollen grain. Besides, there have been sharp declines in sea grasses of some polluted coastal regions [39-40] that may be associated with surface contamination, which, even when the concentration of contaminants is very small, can influence the porous structure of pollen rafts.

The same way it can be explained why a female of some mosquito species (Culex) has to hold onto the egg raft with its hind legs to prevent it from drifting away while she attaches new eggs. The eggs are laid one at a time and stuck together to form a raft that

enables them to float together on the water. If she did not hold onto the raft, it would move away. The eggs of some other mosquitoes (Anopheles) are laid individually onto the water surface; they aggregate under the action of lateral capillary forces with the ends of the eggs touching each other. The spacing between the eggs in this case is relatively larger (which is perhaps advantageous for this species) as they dispersed initially. Lateral capillary forces cause the eggs to cluster and keeps them together while the cluster moves around on the water surface. Traveling in large numbers helps ensure survival of the species, because some of the eggs are eaten by other insects before they hatch.

This relatively-violent phase, when small particles, e.g., flour, pollen, etc., come in contact (Figure 1.4) with a liquid surface, lasts for a short period of time (only about one second or less on mobile liquids like water) and usually followed by a phase that is dominated by attractive lateral capillary forces during which particles slowly come back to cluster. However, once micron- and nano-sized particles are dispersed, they may remain dispersed since attractive capillary forces for them are insignificant. Small particles may experience other lateral forces, e.g., electrostatic, Brownian, etc., which may cause them to cluster or form, patterns [20, 22].

The spreading of solid powders on liquid surfaces and of liquids on solid surfaces are common phenomena that we encounter in our day-to-day life activities such as laundry, lubrication, wet granulation, dyeing and printing, pharmaceutical and food industries [24-25 and 42-43]. Although thermodynamic predictions for liquids spreading over solid surfaces have been developed for many of these applications [44, 45], the mechanism by which solid powders spread over liquid surfaces is not completely understood [46, 47].

1.4 Dissertation Organization

Chapter 2 discusses the transient flow that arises during the adsorption of particles. We explored the cause and nature of the flow for single particle adsorption and multiple particle adsorption cases along with their velocities computed using a flow visualization technique combined with the software PIVlab.

Chapter 3 discusses the application of the adsorption process on liquid interface in botany, understanding the fluid dynamics behind the hydrophilous pollination of a water plant called Ruppia Maritima. Details about the plant and its pollination process and the effect of surface tension on the pollen dispersal mechanism are also presented.

Chapter 4 presents the conclusions in the areas of flow visualization using PIV and hydrophilous pollination.

CHAPTER 2

TRANSIENT FLOW INDUCED BY THE ADSORPTION OF PARTICLES

In Chapter 2, the physics of particle adsorption and the spontaneous dispersion of powders that occurs when they come in contact with a fluid-liquid interface is described along with the experimental set-up and results of our PIV measurements for the transient flow created due to the adsorption of particles. When a particle comes in contact with a fluid-liquid interface it is pulled inwards from the upper fluid into the interface with the lower fluid by the capillary force to its equilibrium position in the interface. It is crucial to understand this motion of the particle in the direction normal to the interface, as it gives rise to the streaming flow on the interface away from the particle.

2.1 Governing Equations and Dimensionless Parameters

The motion of the particle can be obtained by solving the governing equations for the two fluids and the momentum equation for the particle, which are coupled, along with the interface stress condition and a condition for the contact line motion on the particle surface. This is a formidable problem because the capillary force at the line of contact of the three phases on the particle surface depends on the slope of the interface which in general requires the solution of the aforementioned equations [21, 26, 27]. However, a decoupled momentum equation for a particle can be derived by modeling the forces that act on the particle [6, 28]. These forces are: the vertical capillary force (F_{st}), the buoyant

weight (F_g), the Brownian force (F_B), and the viscous drag (F_D). A decoupled equation for the motion of the particle under the action of these forces can be written as:

$$m\frac{dV}{dt} = F_{st} + F_D + F_g + F_B \tag{2.1}$$

where m is the effective mass of the particle which includes the added mass contribution [29], V is the velocity, $F_{st} = 2\pi R\gamma_{12}\sin(\theta_c)\sin(\theta_c + \alpha)$ is the capillary force, α is the contact angle, and θ_c is the particle position in the interface. The Brownian force in Eq. (2.1) is negligible compared to the capillary force [6, 28].

2.1.1 Governing Dimensionless Parameters

Let the characteristic velocity, length and time be given by $U = \gamma_{12}/\mu$, R, and R/U, respectively. Then, Eq. (2.1) can be nondimensionalized to give: see [28]

$$We\, m'\frac{\rho_p}{\rho}\frac{dV'}{dt'} = \sin(\theta_c)\sin(\theta_c + \alpha) + 3V'f_D + \frac{2}{3}B\frac{\rho_p - \rho_c}{\rho}f_b \tag{2.2}$$

Here the primed variables are dimensionless. f_b is the dimensionless buoyancy which is O(1) but depends on the profile of the deformed interface. ρ and ρ_a are the densities of the lower and upper fluids, ρ_c is the effective density of the volume displaced by the particle, and ρ_p is the particle density. The dimensionless parameters in

the above equation are the Weber number $We = \frac{2}{3}\frac{\rho R \gamma_{12}}{\mu^2}$, the Bond number $B = \rho R^2 g/\gamma_{12}$, $\frac{\rho_p}{\rho}$, and the contact angle α. The Weber number is the ratio of inertia forces to capillary forces, and the Bond number is the ratio of gravitational forces to surface tension forces.

For an air-water interface, the parameters have the values: $\mu = 0.001$ Pa.s, $\rho = \rho_p = 1000$ kg/m^3, $\frac{\rho_p - \rho_c}{\rho} = 0.1$ and $\gamma_{12} = 0.07$ N/m. Let us assume that $\mu_a = \rho_a = 0$, m' =1.5, f_d =0.5 and f_b=1. Then, $We = \sim 10^8 R$ and $B = \sim 10^5 R^2$, where R is in meters. Therefore, the role of particle inertia becomes negligible only when R is *much smaller* than 10 nm because only then *We* is much smaller than unity. The influence of gravity becomes negligible when $R < \sim 1$ mm in the sense that such small particles float so that the interfacial deformation is negligible. However, even a negligibly-small deformation of the interface gives rise to attractive lateral capillary forces which, even though small, cause floating particles to cluster. This happens because a particle floating on a liquid surface is *free* to move laterally. The only resistance to its lateral motion is the hydrodynamic drag which can slow the motion but *cannot* stop it. Consequently, only very-small particles, for which lateral capillary forces are smaller than Brownian forces, do not cluster.

2.2 Experimental Setup

The setup consisted of a square Petri dish which was partially filled with Millipore water (see Figure 2.1). The cross-section of Petri dish was 10×10 cm, and the depth was 1.5 cm. PIV measurements were performed in a vertical plane (normal to the camera axis) illuminated by a laser sheet. The vertical position of the camera was in line with the water surface, providing an undistorted view of the volume directly below the water surface. The test particles were dropped on the interface in an area near the intersection of the laser sheet and the camera axis.

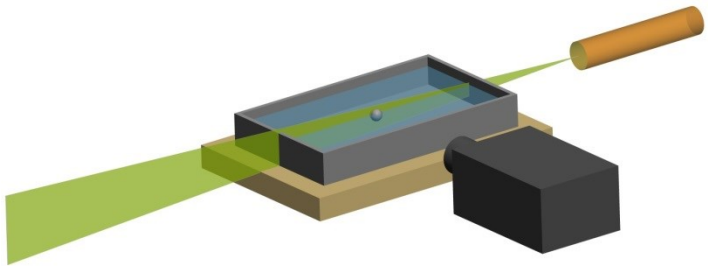

Figure 2.1 Schematic diagram of the PIV experimental setup.

A high-speed camera was used to record the motion of seeding particles visible in the laser sheet. A Nikon 1 series V1 camera equipped with a 30 mm Kenko automatic extension tube and a Tamron SP AF 60 mm 1:1 macro lens was used to provide the required magnification. The laser sheet was generated using a ZM18 series 40 mw solid state diode laser of wavelength 532 nm (green color). Movies were recorded at a resolution of 1280 x 720 pixels. For the particle size range considered (~500 μm to 2

mm), the optimal recording speed for performing the PIV analyses was found to be 60 frames per second. This was determined by a trial and error procedure.

The water was seeded with silver-coated hollow glass spheres of density around 1 gm/cc and average size of around 8-12 μm. The density of seeding particles closely matched the water density, but there was a small particle-to-particle variation. Consequently, some particles sedimented and some rose slowly giving us ample time to record their motion when a flow was induced due to the adsorption of one or more test particles. The seeding particles were silver coated which ensured that the intensity of the scattered light was sufficient to track their motion.

An open-source code, PIVlab, was used for performing the time-resolved PIV analysis. PIVlab is a MatLab-based software which analyses a time sequence of frames to give the velocity distribution for each of the frames. A MatLab code for post-processing and plotting results was written.

2.3 Results

We first discuss our PIV measurements of the transient flow on a water surface that was induced due to the adsorption of a single test particle. Glass particles of three different diameters, 2.0, 1.1, and 0.65 mm were used to obtain the qualitative nature of the flow, and determine how the strength and time duration of the induced flow vary with the particle size.

In agreement with the analytic results obtained in [4], test particles in all cases oscillated vertically before reaching their equilibrium positions in the interface. The frequency of oscillation increased, and the adsorption time decreased, with decreasing particle size in agreement with the analytic results. For example, the frequencies for the diameters 2.0, 1.1 and 0.65 mm were 25 Hz, 50 Hz and 85.71 Hz, respectively.

The adsorption of a test particle caused a flow on the air-water interface, which caused tracer particles trapped on the surface to move away from the adsorbed test particle. Consequently, the water surface near the test particle had few tracer particles which made fluid velocity measurement at and near the water surface difficult. Also, the air-water interface near the test particles was deformed since their density was larger than the water density. In fact, the center of the particles was a fraction of radius below the position of the undeformed interface. The deformation of the interface made viewing of the interface by a camera mounted on a side difficult (see Figure 2.1). Therefore, in our PIV measurements, the velocity was measured only in the region below a horizontal line passing through the point of contact of the interface with the particle which was a fraction of the particle radius below the undeformed interface (see Figure 2.2).

Although the water near the test particle started to move as soon as the particle came in contact with the surface, the adsorption-induced streaming flow intensity developed over a period of time. The intensity reached a maximal strength after a fraction of a second and then it decreased. In the time interval after which the streaming flow reached its maximal strength, the vertical oscillations of the test particle were already negligible. The PIV measurements show that the streaming flow was approximately axisymmetric about the vertical line passing through the center of the test particle (see

Figure. 2.2). Tracer-particles in the region below the test particle moved upwards, and those near and in the water surface moved away from the test particle. The trajectories of fluid particles were qualitatively similar to that for a stagnation point flow, with the center of the test particle being the stagnation point. This implies that the stress on the test particle due to the induced flow was extensional in the horizontal plane near the water surface, and compressive in the direction normal to the surface.

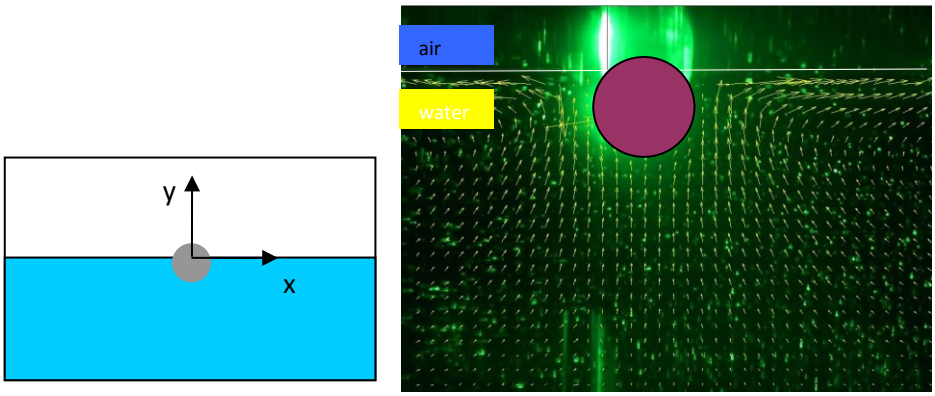

Figure 2.2 (Left) The origin of the coordinate system was at the intersection of the vertical lines passing through the center of the test particle and the horizontal line passing through the point of contact of the interface with the particle. The center of the test particle was a fraction of particle radius below the position of the undeformed interface. (Right) Velocity vectors for the streaming flow induced by a 2 mm test particle 0.67s after it came in contact with an air-water interface. The particle was dropped in a vertical plane illuminated by a thin sheet of laser light. The velocity vectors of tracer particles have been superimposed on the PIV image, and the interface is marked by a horizontal white colored line. A purple-colored mask was used in the PIV analysis to define the region occupied by the test particle. The velocity distribution was approximately axisymmetric about the vertical passing through the center of the particle.

Since the induced velocity field was approximately axisymmetric, it can be conveniently quantified in terms of its y-component along the vertical line passing through the center of the test particle and the x-component along the x-axis as defined in

Figure 2.2. Time was measured from the instant at which the test particle came in contact with the water surface and the distance was measured from the origin of the coordinate system. The former was identified by a frame-by-frame analysis of the movie images. Figure 2.3 shows the y-component of velocity for a 650 μm test particle along the vertical line passing through its center at five different times; the x-component of velocity along this line was relatively small. The y-component of velocity was positive, indicating that the flow was in the upward direction towards the particle. The fluid velocity near the surface of the test particle was small, as the test particle was not moving, and increased with increasing distance from the particle reaching a maximal strength at a distance of about one particle radius from the surface. The velocity then decreased with increasing distance from the particle, but remained significant for a distance of several diameters.

Figure 2.3 also shows that the fluid velocity did not develop instantaneously after the particle was adsorbed. For example, at t = 0.167 s, the maximum velocity of 3.10 mm/s was at a distance of 0.78 mm from the particle, and the velocity at a distance of 5.5 mm was only 0.09 mm/s. The velocity increased with time to reach the maximum value of 8.9 mm/s at t = 0.37 s and y = – 1.04 mm. At y = – 5.5 mm, the velocity at this time was 1.07 mm/s. After reaching the maximum strength, the fluid velocity started to decrease. The decrease first occurred closer to the test particle, while it was still increasing farther away from the particle. For example, the maximum fluid velocity at t = 0.82 s was 7.12 mm/s at y = –1.3 mm, and at t = 1.25 s and y = –1.82 it was 5.47 mm/s. The fluid velocity at larger distances from the particle continued to increase for a longer time interval before starting to decrease. At a distance of y = –5.5 mm, the fluid velocity

at t = 1.58 s was 1.60 mm/s, which was larger than the fluid velocity at this location at t =0.37 s. The streaming flow slowly reduced in strength but continued for several seconds.

Figure 2.4 shows the x-component of fluid velocity for a 650 μm test particle along a horizontal line at five different times; the y-component of fluid velocity along this line was negligible. The velocity was positive which means that the water near the surface was moving away from the particle. As in Figure 2.3, the fluid velocity near the test particle was small because it was not moving, and increased with increasing distance from the particle and then after reaching a maximal value it decreased with increasing distance. However, the maximal fluid velocity was at a distance of about two particle diameters from the particle surface, whereas below the particle the maximum was reached at a distance of one particle radius. The velocity remained significant for a distance of several diameters. The maximum water velocity near the surface was comparable to the maximum velocity below the test particle.

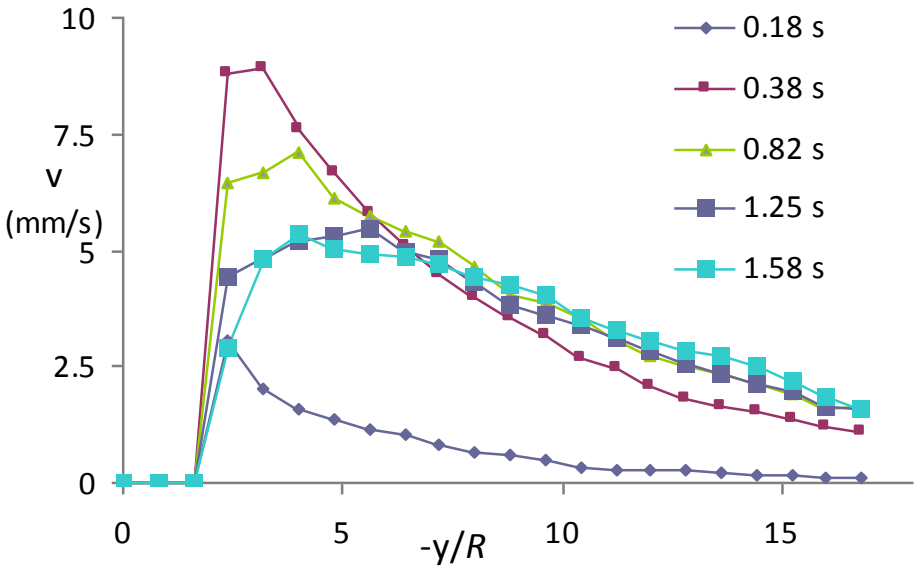

Figure 2.3 Temporal evolution of the streaming flow induced by the adsorption of a 650 µm particle. The fluid velocity is shown at five different time intervals after the test particle came in contact with the water surface. The vertical component of fluid velocity (v) is shown as a function of *-y/R*.

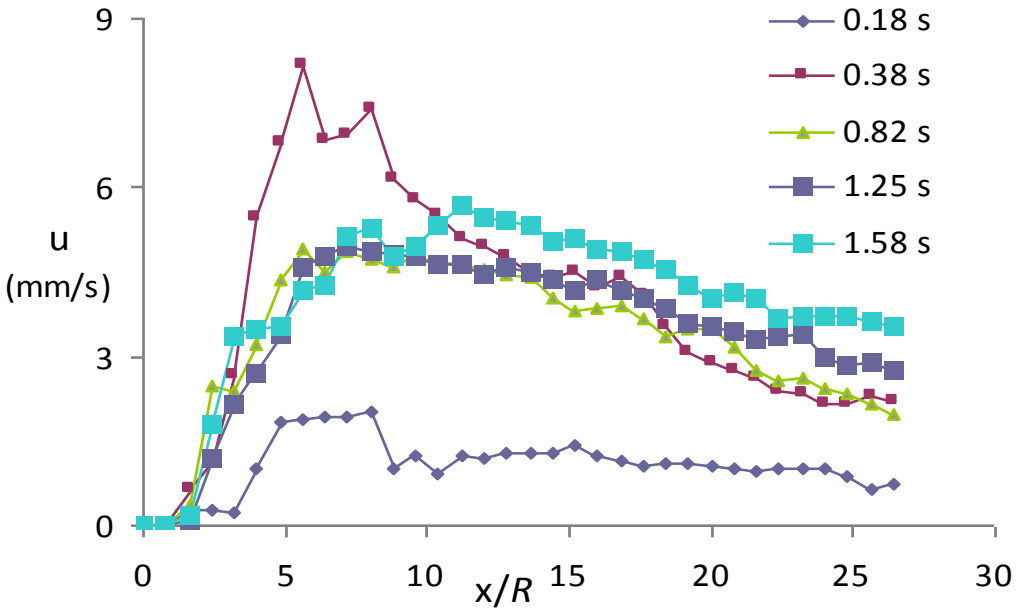

Figure 2.4 Temporal evolution of the streaming flow induced by the adsorption of a 650 µm particle. The fluid velocity is shown at five different time intervals after the test particle came in contact with the water surface. The horizontal component of fluid velocity (u) is shown as a function of *x/R*.

The temporal evolution of streaming flow near the water surface was qualitatively similar to that in the water below the test particle. The flow started when the particle touched the water surface, and reached a maximal value after a time interval which was comparable to that below the particle. At t = 0.167 s, the maximum velocity of 1.91 mm/s was at a distance of 2.1 mm from the particle, and the velocity at a distance of 5.5 mm was 1.1 mm/s. The velocity increased with time to reach the maximum value of 8.2 mm/s at t = 0.37 s and x = 1.82 mm. At this time, the velocity at x = 5.5 mm was 4.4 mm/s. This shows that the velocity near the water surface was more intense over a larger area than below the particle. The strength of the streaming flow then decreased with time with the decrease first occurring closer to the test particle.

The time interval after which the streaming flow attained the maximal intensity and the volume over which the flow extended varied with the particle size. The velocity distribution for a 2 mm particle is shown Figure 2.5. The figure shows that the streaming flow evolution was qualitatively similar to that for a 650 μm particle described above. However, it developed relatively more slowly. The maximum velocity of 13.5 mm/s was reached 1.58 s after the particle came in contact with the water surface. For a 650 μm particle, on the other hand, the maximal velocity was reached at t = 0.38 s. For a 2 mm particle, not only the maximum velocity was larger, it occurred at a larger distance of 1.38 mm from the test particle, and so the volume over which the flow was intense was larger than for a 650 μm particle. Our PIV measurements of the three particle sizes considered show that the time interval after which the maximal flow strength was attained, the volume over which the flow intensity extends, as well as the time interval for which the flow persists, increase with increasing particle size.

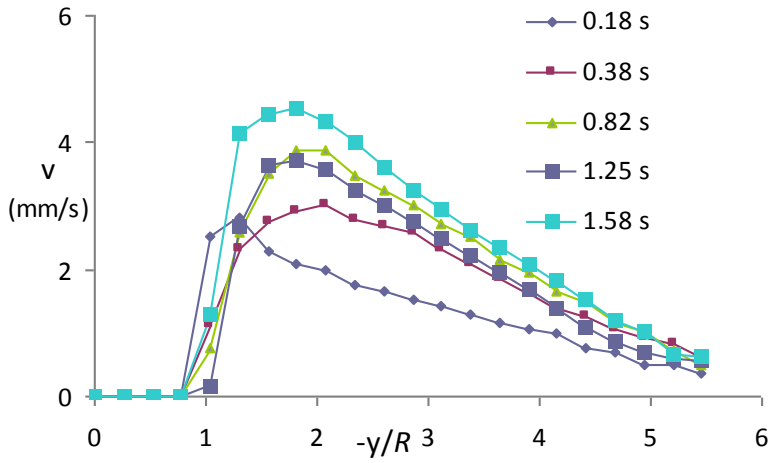

Figure 2.5 Temporal evolution of the streaming flow induced by the adsorption of a 2 mm particle. The velocity is shown at five different time intervals after the test particle came in contact with the water surface. The vertical component of velocity (v) is shown as a function of $-y/R$.

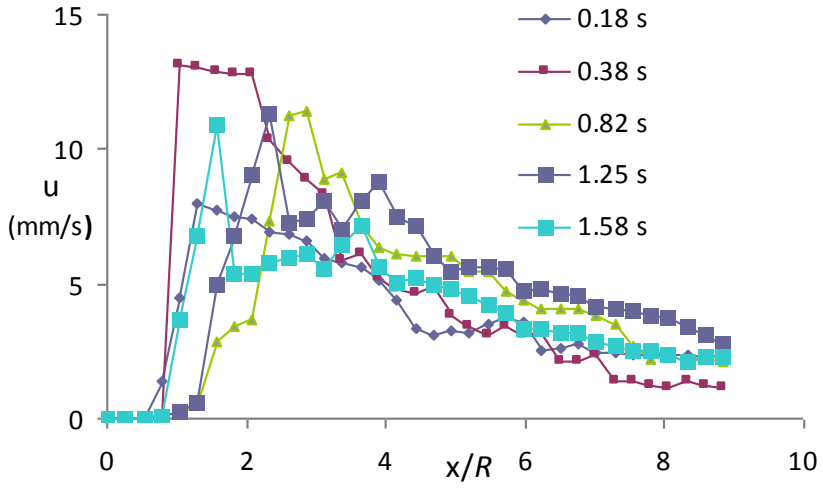

Figure 2.6 Temporal evolution of the streaming flow induced by the adsorption of a 2 mm particle. The velocity is shown at five different time intervals after the test particle came in contact with the water surface. The horizontal component of velocity (u) is shown as a function of x/R.

2.3.1 Adsorption of Two or More Particles

We next consider the case in which two 650 μm particles were simultaneously adsorbed at an air-water interface. The particles were dropped onto the interface such that the line joining their centers was in the plane of the laser sheet. This ensured that the induced flow was approximately symmetric about the vertical plane passing though the centers of the two particles, and also about the vertical plane bisecting the line joining their centers. Figure 2.7 shows that each of the particles induced a streaming flow which was similar to that which was induced by a single particle. The combined flow below the particles was in the upward direction and near the water surface the flow was away from the particles. In the region between the particles, the horizontal flow contributions approximately cancelled and the vertical contribution added. Thus, the combined streaming flow was approximately the sum of the flows induced by the two particles individually and thus stronger than the flow induced by one particle. The combined flow developed in about 0.4 s which was comparable to the time in which the streaming flow developed for a single 650 μm particle.

For the case shown in Figure 2.7, the two particles were initially close to each other and so the streaming flow induced by the first particle caused the second one to move away, and vice versa. The symmetry of the streaming flow with respect to the laser sheet ensured that the two particles remained in the plane of the laser sheet while they moved apart. However, when the particles were dropped so that the angle between the line joining their centers and the laser sheet was not small, the streaming flow carried them away out of the plane of the laser sheet, and so they were visible only for the time duration for which they were illuminated. The speed at t =0.167 s was approximately

12.3 mm/s. The speed decreased as they moved farther apart, and also with time as the streaming flow intensity diminished with time. In fact, after the distance between them was about 10R their speeds became negligible.

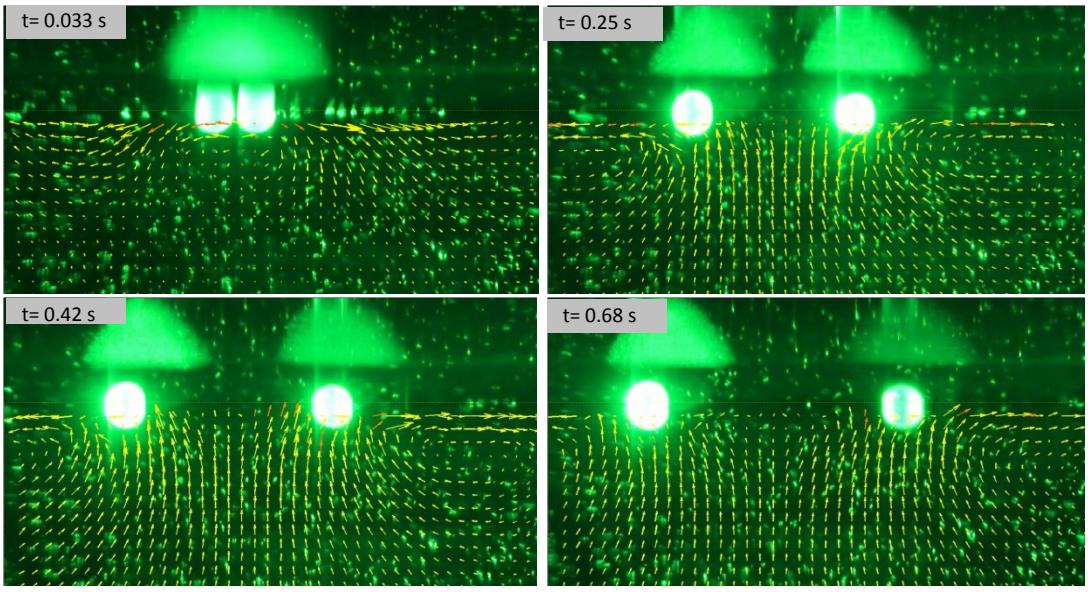

Figure 2.7 The figure shows the streaming flow induced by two 650 μm test particles after they came in contact with an air-water interface. The particles were dropped in a vertical plane illuminated by a thin sheet of laser light. The velocity vectors have been superimposed on the PIV images. The flows induced by the particles caused them to move apart. The size of velocity vectors is arbitrary, and for clarity a larger magnification is used in the plot at t=0.033 s than in the later plots.

We also considered cases where about 10-30 particles were dropped onto an air-water interface in and near the laser sheet (see Figure 2.8). Again, each of the particles induced a streaming flow in the water that was similar to the flow induced by a single particle. These flows induced by the particles caused neighboring particles to move away, and so the net result was that particles moved radially outward from the location where they were dropped. Experiments show that clusters of particles disperse radially outward from the center (see Figure 1.1 which shows streak lines), and that when the cluster size was larger, the radius of the approximately-circular area over which its particles

dispersed and the dispersion velocity were larger. This increase in the dispersion velocity with an increasing number of particles was also seen in our direct numerical simulations [6]. The PIV measurements show that the water rises in the region where particles were dropped, and on the surface it moved away from this region.

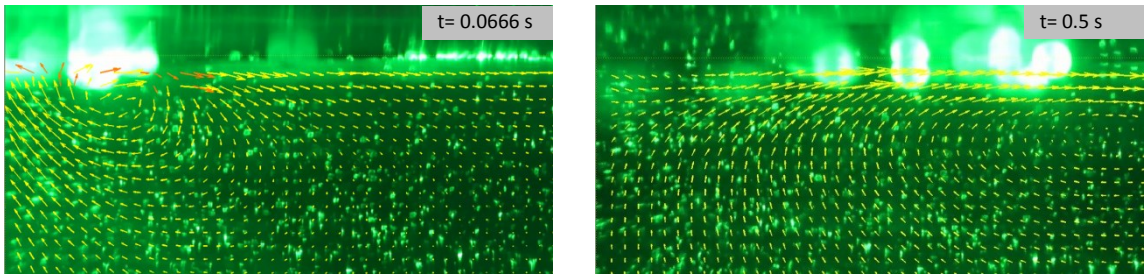

Figure 2.8 The figure shows the streaming flow induced by about 20, 650 µm particles after they came in contact with an air-water interface. The particles were dropped in and near a vertical plane illuminated by a thin sheet of laser light, and towards the left side of the photographs. The figure shows the motion of the particles that moved to the right side (some of the particles moved in other directions and so are invisible in the photographs). The velocity vectors have been superimposed on the PIV images. The size of velocity vectors is arbitrary.

2.4 Conclusion

When a particle comes in contact with a fluid-liquid interface the vertical capillary force pulls it into the interface which gives rise to a transient streaming flow. The PIV measurements show that the liquid below a newly-adsorbed particle rises upwards and the liquid near the surface moves away from the particle. The induced flow for a spherical particle was axisymmetirc about the vertical line passing through the particle center. Also, the flow strength is not established immediately after the particle comes in contact with the interface, but builds up over a short time interval. For a 650 µm glass sphere the maximum flow strength occurred about 0.4 s after the particle come in contact, and for a 2 mm sphere after about 1.5 s. We also considered 1.1 mm, 0.85 mm and 0.55 mm glass spheres for which the maximal flow strength occurred after 0.75 s, 0.47s and

0.18 s, respectively. These results show that the time interval after which the maximal flow strength occurred decreased with decreasing particle size.

When two or more particles were simultaneously adsorbed, the streaming flow was a combination of the flows induced by the particles individually and so the flow strength increased with increasing number of particles. Consequently, the distance travelled by the particles near the outer periphery of a cluster sprinkled on a liquid surface can be several orders of magnitude larger than any dimension of the area over which the particles were sprinkled. This can be important for some physical processes occurring on a water surface, such as the pollination of hydrophilous plants, and the transportation and rate of spread of microbes and viruses on a water surface. Furthermore, the streaming flow can break apart agglomerates of particles when they are adsorbed at a fluid-liquid interface which is important in various processes in the pharmaceutical and food industries such as wet granulation and food processing.

CHAPTER 3

FLUID DYNAMICS OF HYDROPHILOUS POLLINATION IN *RUPPIA* (WIDGEON GRASS)

In this chapter, the physics underlying the mechanisms of two-dimensional aquatic pollen dispersal, known as hydrophily is presented. This has evolved in several genera of aquatic plants, including *Halodule*, *Halophila*, *Lepilaena*, and *Ruppia*. We selected *Ruppia maritima*, which is native to salt and brackish waters circumglobally, for this study.

3.1 Introduction

Hydrophily or hydrophilous pollination is the type of pollination where water is the medium. Some examples of hydrophily plant genus are Halodule, Halophila, Lepilaena, and Ruppia. *Ruppia maritima* L., commonly known as widgeon grass, is a species of sea grass belonging to the family of Ruppiaceae. It is globally distributed in temperate and tropical regions. *R. maritima* occurs in brackish waters as well as in continental sea waters and also in hyperhaline waters, where it can tolerate salinities up to 3 times the salinity of the sea. In the U.S, it occurs in brackish waters along Atlantic coast as well as in alkaline ponds and streams. The plant is categorized as hermaphrodite.

The pollination in this plant occurs on water surface. In *Ruppia,* the transport of pollen from an anther to a stigma takes place primarily on a water surface(surface pollination) [9, 30]. It has been reported that under-water pollination (hypohydrophilous) may also occur in the plant [87]. It was noted that ‘under-water pollination and surface

pollination are mutually exclusive adaptions [90]. The possibility that both mechanisms may function in same population under different environmental conditions remains unverified [90]'. As such the pollination process is two-dimensional (see Figure 3.2). The density of pollen grains is higher than that of water and so a mechanism is needed for transporting them to the water surface where they become trapped at the air-water interface. If they are not adsorbed on water surface they quickly sediment away from stigmas, which are generally present at or near the water surface. In fact, to facilitate pollination, matured stigmas position themselves so that they are at the water surface during low tides (see Figure 3.1).To model the transport process, we need to understand the mechanisms by which the pollen grains from an anther are adsorbed in the water surface and the hydrodynamic forces that govern their subsequent motion in the surface toward the stigma. Our objective is also to study the role of surface tension in the transport process and how it is affected by the presence of surfactants that may be present because of water contamination.

a b

Figure 3.1 (a) *Ruppia maritima* growing in a lagoon at the Jersey Shore. The photograph was taken during low tide. (b) Stigmas floating at the water surface.

It is well known that particles trapped in liquid surfaces interact with each other via lateral capillary forces, which arise because of their weight, to form clusters or monolayer arrangements [5, 6, 31]. A common example of capillarity-driven self-assembly is the clustering of breakfast-cereal flakes floating on the surface of milk. The deformation of the interface by the flakes gives rise to lateral capillary forces that cause them to cluster. This, as discussed below, is also the mechanism by which pollen particles cluster together to form pollen rafts. In recent years, many studies have been conducted to understand this behavior of trapped particles because of their importance in a range of physical applications and biological processes e.g., formation of insect egg rafts, stabilization of emulsions, and self-assembly of particles at fluid-fluid interfaces to form novel nano-structured materials that can be used in anti-reflection coatings for high-efficiency solar cells, photonic crystals and biosensor arrays.

Our observations concur with previous studies [10, 87] on pollination process in *Ruppia maritima.* An anther can release its pollen either below or above the water surface depending on its position relative to the water surface, and, in some cases, it can release the pollen right at the surface when it is in contact with the water surface. Before they are released from the anther, the pollen grains are clumped together in a kidney-shaped mass; when the mass comes in contact with the water surface, its pollen partially disperses on the surface. The dispersion occurs in two-dimensions, i.e., on the water surface, in the sense that a significant fraction of the pollen grains are adsorbed at the surface. The pollen grains which are not adsorbed at the surface slowly sediment to the bottom as they are slightly denser than water. Pollen dispersion on the surface is a crucial first step in the formation of floating porous pollen structures called “pollen rafts.” Specifically, our

experimental observations show that the dispersion causes the pollen grains from an anther to spread on the water surface into an approximately oval-shaped region which contains a densely packed layer of pollen grains in the middle and a surrounding monolayer of grains. Several of these dispersed clusters subsequently join together under the action of lateral capillary forces to form a pollen raft. A pollen raft often contains pollen grains from several anthers.

Clusters and rafts of pollen adsorbed in a water surface are subjected to hydrodynamic drag and capillary forces. The vertical component of capillary force keeps them afloat, and its lateral component moves them tangentially on the water surface. A depression in the water surface created by a stigma gives rise to a lateral capillary force that transports the pollen toward the stigma. The latter is the key mechanism that enhances the probability of pollination, which is especially important because these plants produce pollen in limited quantities in comparison to the plants that rely on three dimensional pollination [30].

Flow on the surface of oceans or lakes changes with changing wind and water currents. Therefore, in addition to lateral capillary forces, floating pollen grains and rafts are subjected to hydrodynamic forces that arise because of surface flow. This makes an experimental study of the role of capillary forces in the pollen transport process difficult to carry out under natural conditions. We, therefore, decided to conduct experimental studies of the adsorption and transport of pollen on the water surface under controlled laboratory conditions. Specifically, we tested the following hypotheses**:**

1. Pollen can be released above or below the water surface depending on the water level which changes during tides (see Figure 3.2).

2. Pollen released below the surface is transported to the water surface by gas bubbles, and pollen released above the surface simply falls onto the water surface.

3. When a pollen mass comes in contact with the water surface it partially disperses on the water surface which increases its boundary length and this increases the vertical capillary force which keeps it afloat.

4. Partially dispersed pollen masses cluster under the action of lateral capillary forces to form pollen rafts.
5. Stigma positions itself on the water surface depressing the surface which gives rise to lateral capillary forces that transport pollen rafts towards the stigma. The above processes can be disrupted by adding surfacta nt as the surface tension of water is reduced.

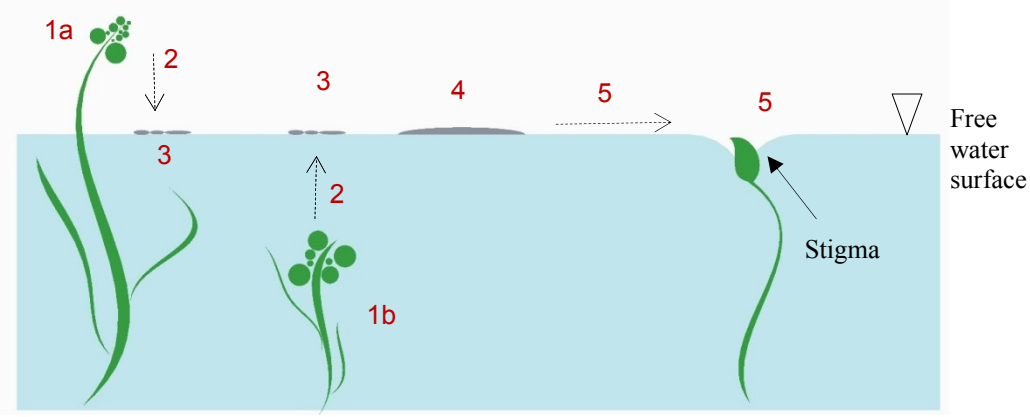

Figure 3.2 Schematic of pollination process.

3.2 Experimental Methodology and Results

For the last three years, we have collected *Ruppia maritima* from the north coast of Long Island and the Jersey Shore just as it was coming into bloom. This was the optimal condition in which to manipulate and observe pollen release and its interaction with the water surface. Field samples of male and female flowers along with the water from the site were collected for experimentation, and whole plants in their native soil were transferred to saltwater aquariums at Brooklyn Botanic Garden and the New Jersey Institute of Technology for observation. For most part of the experiments, we used the

plants collected from Barnegat Bay, near the town of Lavallette, Ocean County in New Jersey. The plants were up to 2.5 feet long and were densely distributed (15-20/sq.m) on the collection site's sandy substrate.

We dissected anthers to study the structure of the contained pollen and to estimate the effective density of pollen clusters of various sizes (see figure 4). We found that the size of *Ruppia* pollen grains is about 40 microns, and the average density of pollen cluster (1.024 g/cm^3) is slightly higher than the density of brackish water (1.016 g/cm^3) and sea water (1.023 g/cm^3). The density was estimated by measuring the sedimentation velocity of pollen clusters of four different sizes (0.48 mm, 0.65 mm, 0.83 mm and 0.91 mm) which were of approximately spherical shape. Specifically, the sedimentation velocity varied between 0.125 and 0.363 cm/s which was used to calculate the Reynolds number (which was found to be around unity). Then the drag coefficient was obtained and it was used to calculate the drag which was then equated to the buoyant weight and the resulting equation was solved for the effective density of the pollen clusters. The estimated density varied between 1.022 and 1.025 g/cm^3, and the average value was 1.024 g/cm^3.

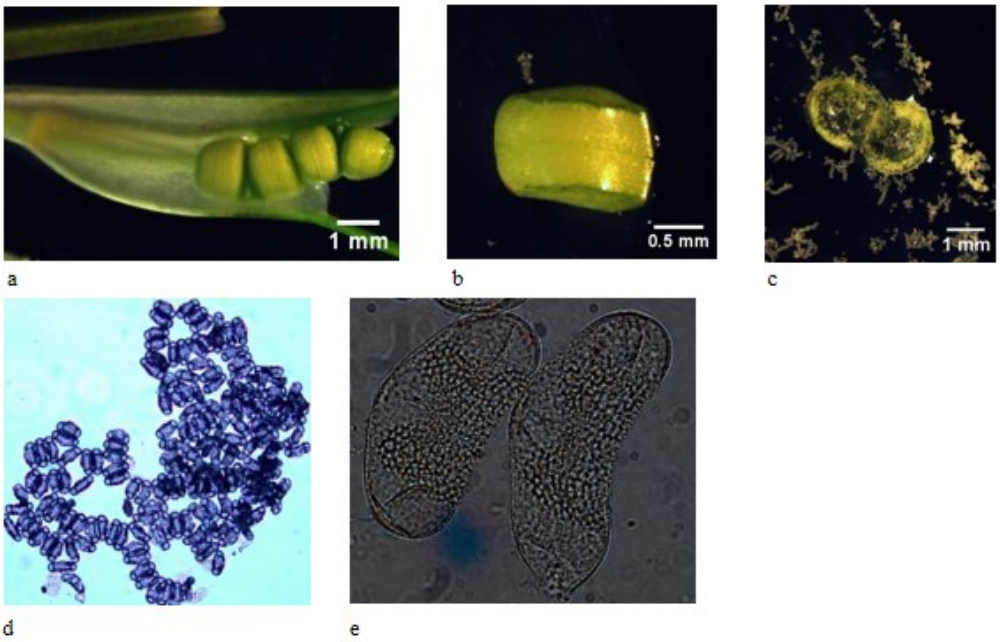

Figure 3.3 Anthers and pollen grains of *Ruppia*. (a) Male flower (anthers); (b) close-up view of one anther; (c) Anther cut open with pollen grains on liquid surface; (d) Magnified view of pollen grains in 100x; (e) Magnified view of pollen grains in 1000x.

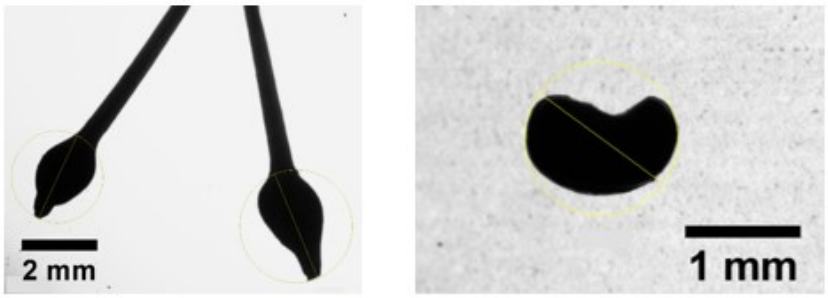

Figure 3.4. Scaled images of stigma and anther of *Ruppia.*

The water we collected from the site has salinity (22 parts per thousand), less than that of sea water (35 parts per thousand) and more than that of fresh water, so it is considered to be brackish water. We shall continue to refer to this native brackish water as native water whenever required from here forward. Under natural conditions, male inflorescences can be above, below or in contact with the water surface, and this may change for an inflorescence as the water level varies during tides. We conducted our

experimental studies of the adsorption and transport of pollen in this plant on the water surface under controlled laboratory conditions. Therefore, in our experiments we placed the male inflorescences in the beakers so that they were a few millimeters above, below and near the water surface. The roots of the plants were kept immersed in the water collected from the site from where the plants were harvested. The cameras mounted above and on the sides of the beaker continuously recorded at 60 fps (frames per second) the anthers in inflorescences as they matured and their pollen was released. The pollen travelled to the water surface and was adsorbed at the surface, and subsequently travelled laterally on the surface toward the stigma.

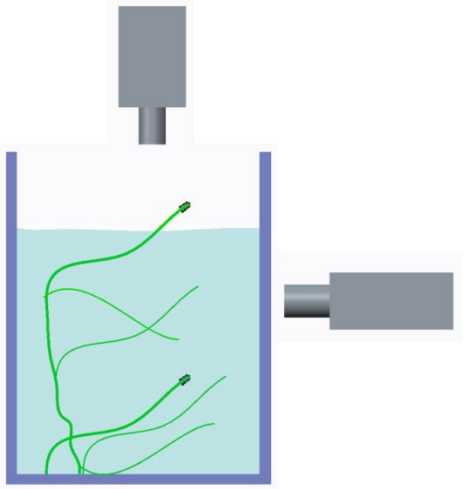

Figure 3.5 Schematic of our experimental setup with cameras recording the motion of pollen from top and side.

3.2.1 Anthers Below the Water Surface

We first discuss the cases in which the stems containing anthers were placed a few millimeters below the water surface. Since the density of pollen and its clumps is slightly larger than the density of water, a mechanism is required to carry them to the water surface *without* wetting so that they can be adsorbed and kept floating by the vertical capillary force. Our video recordings show that when an anther dehisces, it releases gas

bubbles, which attach to the pollen mass making it buoyant. It is likely that the bubbles contain lacunal gas that is present in aquatic plants [30, 34-35]. During this process, some pollen grains broke loose from the pollen mass and were adsorbed on the surface of the bubble. Subsequently, the pollen mass detached from the anther, but remained largely intact as it was carried to the water surface by the gas bubble along with the pollen grains that were adsorbed on the surface of the bubble. The pollen mass erupted from the enclosing green anther sac in some cases, leaving the anther sac attached to the plant and, in other cases, the anther sac rose to the interface with the pollen mass attached to the gas bubble.

After reaching the water surface, in most cases, the bubble popped and the pollen mass dispersed immediately, and the pollen was adsorbed at the water surface. In other cases, the pollen mass and the bubble remained intact for a time interval ranging from a few seconds to several minutes (see Figures 3.6-3.8). For example, the pollen mass in Figure 3.6 dispersed after 15 seconds and that in Figure 3.7a after 24 minutes. The pollen mass was attached to the bottom portion of the bubble (which was below the water surface) such that the center of mass of the pollen mass was below the center of the bubble (see Figure 3.7b). The precise mechanism by which the bubbles popped and the pollen mass dispersed at the surface was not clear from the videos as this happened very quickly; the time taken was smaller than the time interval of 1/60 sec between two consecutive frames. Our frame-by-frame analysis shows that some of the pollen grains became airborne and travelled as much as a few millimeters away from the pollen mass before falling back onto the water surface (see Figure 3.7d). The fact that some of the pollen became airborne indicates that as the bubble burst, the gas trapped inside the

bubble or the motion induced at the interface, or both, imparted momentum to the pollen mass.

The dispersion of pollen mass was partial in the sense that it spread into an approximately oval-shaped region that contained a densely packed white colored cluster of pollen grains in the middle that was surrounded by a thinner annular grey colored layer (see Figure 3.6h). The color is related to the local vertical thickness of the pollen layer, when the thickness is smaller the color is darker and when it is larger the color is more whitish. For example, the outer annular region of dispersed pollen mass in Figure 3.6h was darker because the thickness was smaller. The qualitative structure of the partially dispersed pollen masses was independent of the bubble that carried it to the interface, i.e., they all contained a white colored core that was surrounded by a grey colored annular region. The area of the outer annular region however varied. The annular layer was loosely attached to the inner dense core. Thus, in some case, parts of annular layer broke apart because of the air currents in the room that caused the water to swirl resulting in hydrodynamic shearing forces which caused loosely attached portions of the annular layer to break apart.

Notice that the length of the outer boundary of the partially dispersed pollen mass in Figure 3.6h is nearly ten times longer than that of an undispersed pollen mass in Figure 3.6i. As discussed in Appendix A, the maximum vertical capillary force on a body depends on the length of its boundary along which the interfacial tension acts [6]. Therefore, the increased boundary length of a pollen mass because of the dispersion increases the maximum vertical capillary force that can act on the pollen mass, allowing it to float on the surface without sinking.

Several partially dispersed pollen masses attracted each other to form pollen-rafts, which often contained clumps from several different anthers (see Figure 3.8c). Lateral capillary forces among floating pollen masses were significant because of their relatively large size and thus a newly released pollen mass would quickly merge with the raft. The time taken to merge depended on the initial distance. For example, when the distance was around 5 cm they merged in about one minute.

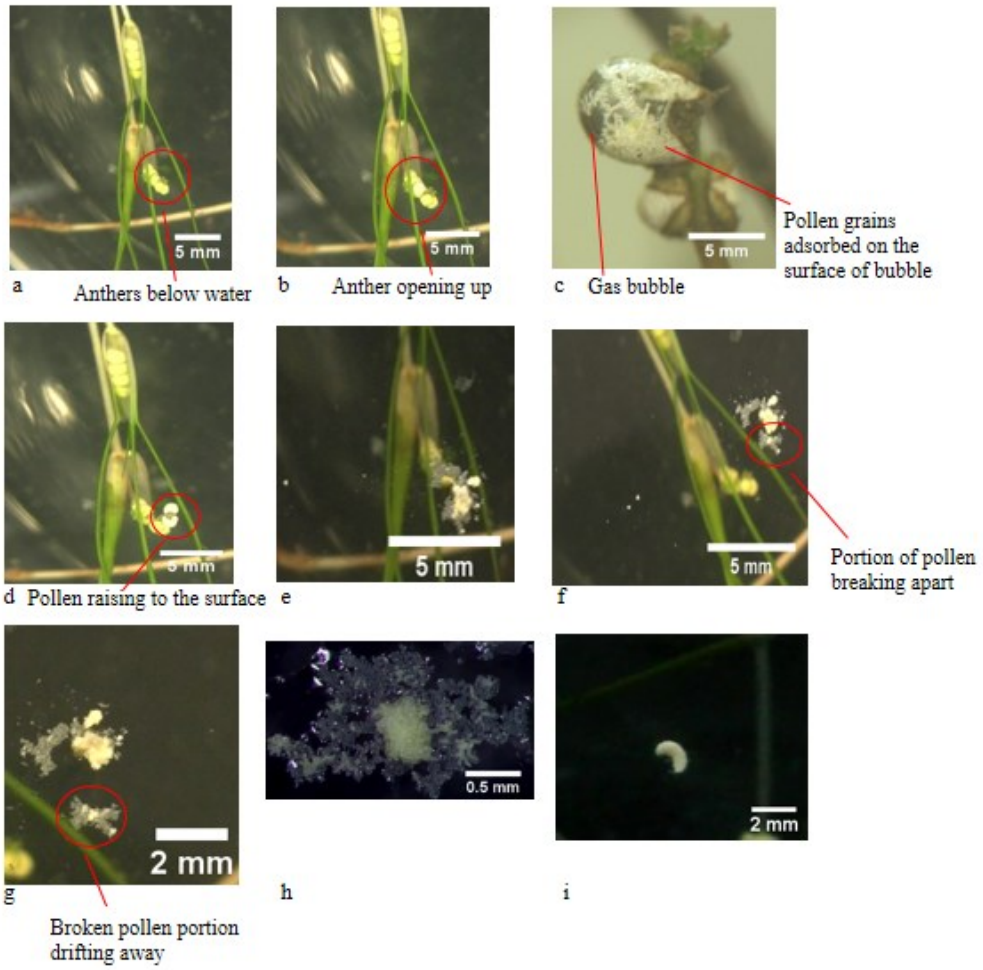

Figure 3.6 Pollen mass released from anthers below the air-water interface disperses upon reaching the interface. In most cases, it dispersed immediately after coming in contact the surface: (a) Anther pods, before opening, (b) An anther is opening up, (c) An air bubble with pollen grains and pollen mass adsorbed on its surface, (d) A pollen mass rising to the water surface (side view), (e) A partially dispersed pollen mass, (f) A portion of the monolayer surrounding the pollen mass is breaking apart, (g) Close up of partially dispersed pollen mass, and (h) A portion of monolayer has broken apart from the core of the partially dispersed pollen mass.

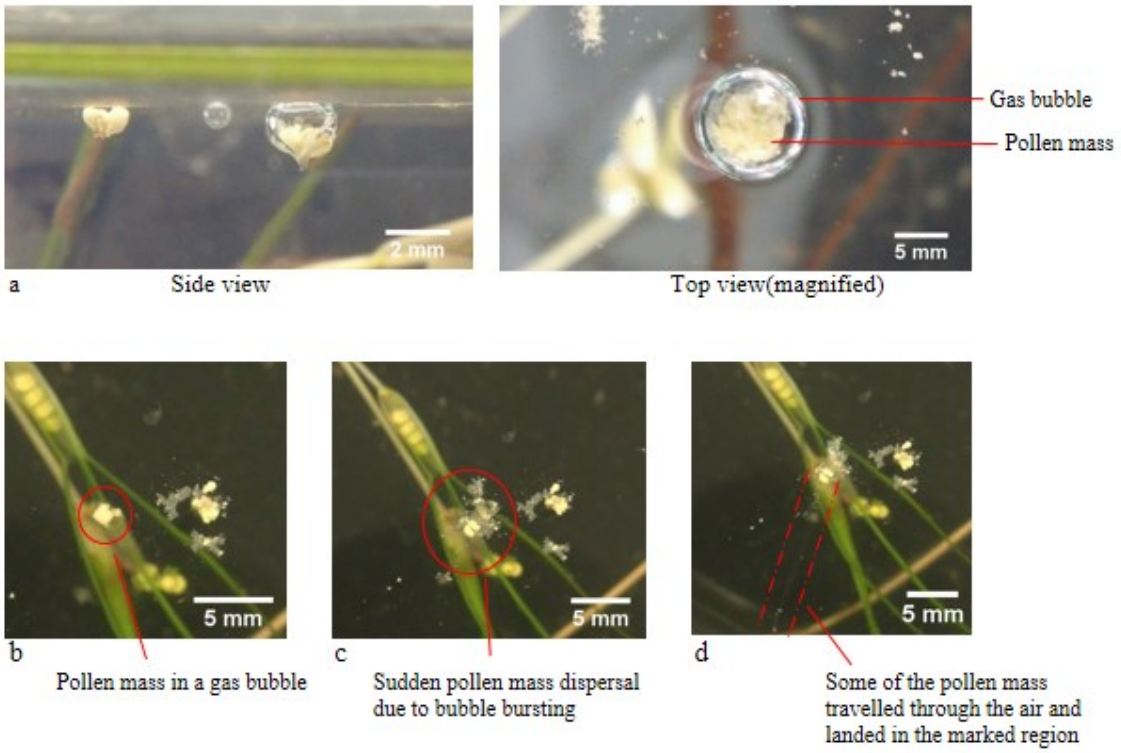

Figure 3.7 Pollen mass with air bubble dispersed (a) pollen mass with air bubble remained intact for 24 minutes (b) The pollen mass dispersed and the bubble burst at the same approximate time (c-d) show the dispersion of pollen mass as the bubble burst. Notice that some of the pollen became airborne.

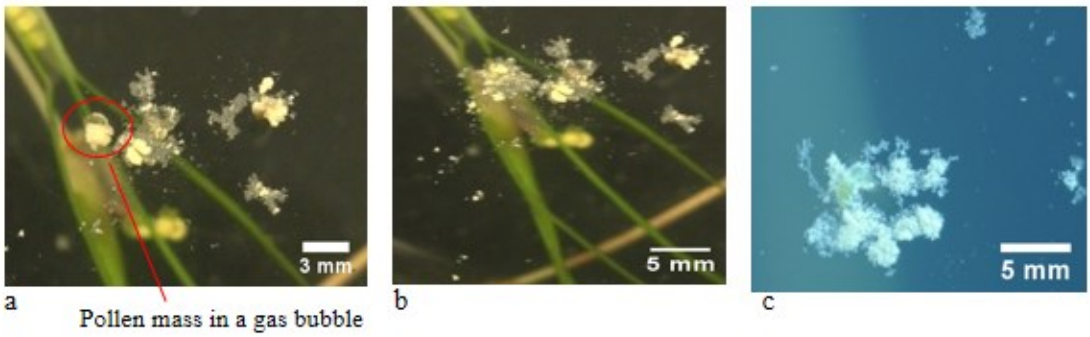

Figure 3.8 Pollen mass with air bubble dispersed (a) Pollen mass with an attached bubble (marked by a circle) (b) Bubble has burst and the pollen mass dispersed (c) Several dispersed pollen mass forming pollen raft

3.2.2 Anthers Above Water Surface

We next discuss the cases where the top portion of plants containing anthers were placed a few centimeters above the water surface. The plants were sufficiently long such that their stems remained immersed in the water. Here, after detaching from the anther, the pollen mass simply fell onto the water surface. Our video recordings show that the cohesive forces holding the grains of the pollen masses clustered varied significantly. In some cases, the grains were so loosely attached that the pollen mass appeared powdery (see Figure 3.10). The dispersion behavior in these cases was similar except that the pollen dispersed over a larger area. At the other extreme the pollen mass broke into only a few pieces before coming in contact with the water surface as in Figure 3.9. We believe this variation in the behavior is due to the maturity level of the pollen.

For the latter type of cases we observed that although the pollen masses remained essentially intact while falling onto the water surface, some smaller pieces broke away from the main part while breaking away from the anther or while in the air and landed nearby. The intact pollen masses partially dispersed immediately after coming in contact with the water surface, and then interacted with each other to form pollen rafts (see Figure 3.9). These rafts were similar to those formed by the pollen released below the water surface.

The dispersed pollen masses attracted other pollen masses floating on the surface to form a pollen raft. Due to their relatively larger size, they clustered relatively quickly to form pollen rafts. The time taken by a newly released pollen mass to cluster with the raft depended on its initial distance from the raft. For example, a typical pollen mass

merged with a raft 5 cm away within one minute. The speed with which it travelled increased as it approached the raft.

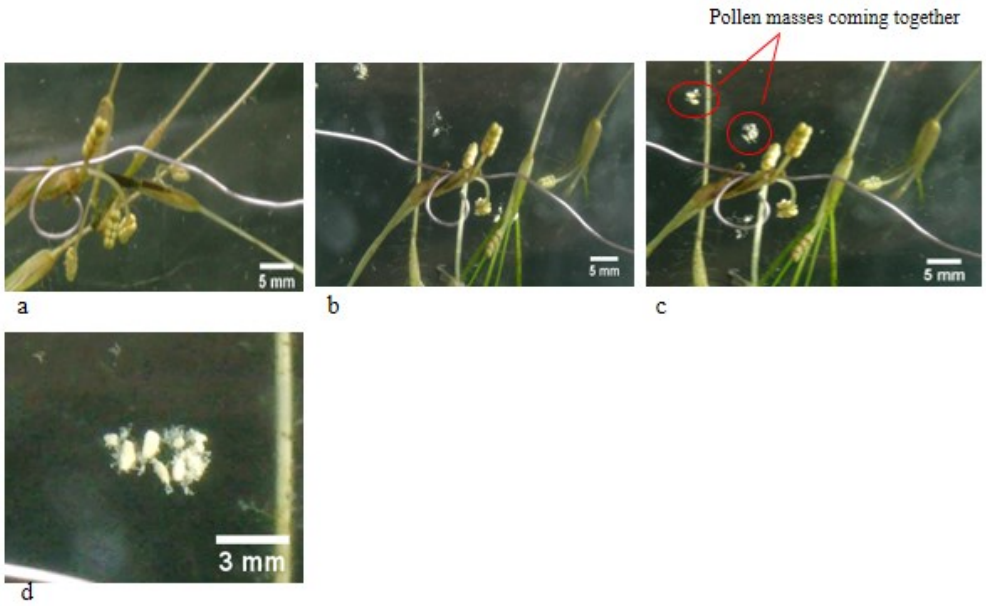

Figure 3.9 The figures (a-d) show pollen masses released above the water surface. The pollen masses landed essentially intact on the water surface but some small portions broke apart in the air. Pollen masses came together to form pollen raft.

Figure 3.10 The figures (a-c) show pollen masses released above the water surface. The pollen masses fell in fine powdery form of pollen even as they were travelling from air to water.

3.2.3 Lateral Migration of Pollen Rafts and Pollination

As discussed in Appendix B, particles denser than water can remain trapped on the water surface because of the vertical capillary forces that arise because of the deformation of water surface around the particles. The deformation also gives rise to lateral capillary forces that move them on the surface towards a local surface depression where they get collected. This is the key transport mechanism by which *Ruppia* pollen travels laterally on water surface. It is noteworthy that the capillary force between two floating particles varies as the product of their buoyant weights, and so the force varies as the second power of the density difference and the third power of the product of their sizes or radii. For pollen grains the density mismatch was small as their density was only slightly larger than the water density and their size is about 40 μm. The capillary force between pollen grains was in fact comparable to the Brownian force and so was not large enough to cause them to cluster [3,4]. Therefore, lateral capillary forces can efficiently transport pollen towards a surface depression (created by a stigma) only when the buoyant weight of the search vehicle is sufficiently large and this can happen only when they first form pollen rafts (see Appendix B).

When matured stigmas positioned themselves on the water surface such that their openings were at the surface, that caused the water surface to depress around the openings (see Figure 3.11). Pollen rafts deformed the surface substantially more than a single pollen grain because of their larger size and buoyant weight and so were strongly attracted to the surface depressions created by the stigmas and collected around such openings of the stigmas. The formation of pollen rafts thus increases the probability of pollination.

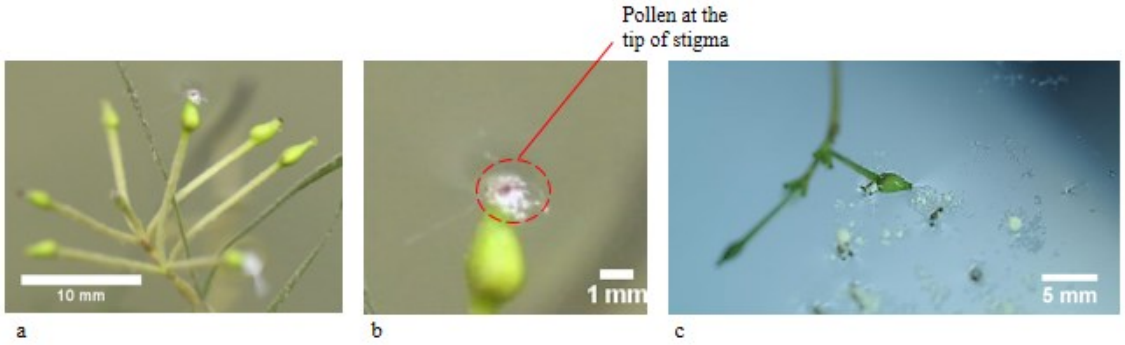

Figure 3.11 A female florescence at a water surface with two of its stigmas in contact with the water surface. (a) Female inflorescence, and (b-c) Magnified views of the stigmas in contact with the water surface. Notice the white colored pollen that is connected at their openings.

3.3 Pollen Dispersion on Pure Water

To study the role of native water's salinity in the dispersion of pollen masses, we placed the plant stems in native water and the anthers were placed so that the pollen mass would fall into another container that was filled with pure water (pure deionized water obtained from a Milli-Q system). The initial picture in Figure 3.12 shows pollen mass that fell onto the pure water surface in powdered form. It continued to disperse and after a few hours completely broke apart into a monolayer. Figures 3.9 and 3.10 show a similar pollen mass that fell on native water and dispersed partially. This shows that native water inhibits the breakup of pollen mass into a monolayer. Since pollen masses disperse only partially on the native water, they can cluster together under the action of lateral capillary forces. Completely dispersed monolayers of pollen, on the other hand, do not cluster since lateral capillary forces for them are small.

To further study this matter, we studied the dispersion of pollen clumps under the microscope by dropping them on the surface of water in a petri dish. The pollen clumps in this experiment were the pollen masses that were captured on a microscope slide as they fell from the anthers. When a pollen clump was dropped on to the surface of native

water it dispersed only partially (see Figure 3.13a). But, when a pollen clump was dropped on pure water surface it dispersed completely into a monolayer which contained long chains (see Figure 3.13b). These results show that the properties of native water also play an important role in the formation of pollen rafts. On native water pollen clumps disperse only partially and several of them combine to form pollen rafts which does not happen on pure water.

Figure 3.12 Dispersion of pollen mass on the surface of pure water. The pollen mass partially dispersed when it came in contact with the surface. It continued to slowly disperse and after 05 hours, it dispersed into a monolayer of pollen grains and some small clumps.

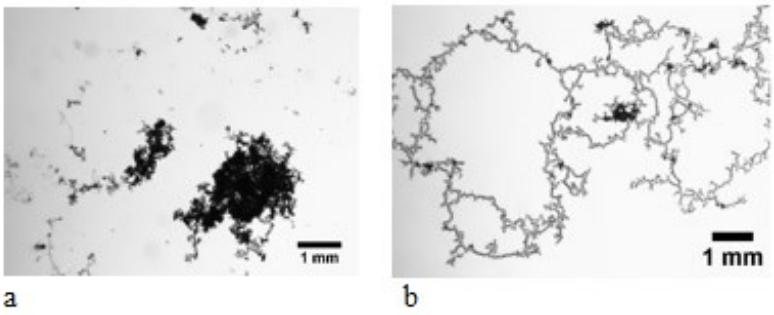

Figure 3.13 Dispersion of pollen clumps observed under microscope. (a) The pollen clump dispersed only partially on the surface of native water. (b) The pollen clump completely broke apart on the surface of pure water into a monolayer of chains.

3.4 Pollen in Surfactant Contaminated Native Water

As described above, surface tension plays an important role in hydrophilous pollination. It causes pollen masses to partially disperse when they are adsorbed at the water surface, increasing the vertical capillary force which is essential for keeping them afloat. Also, it gives rise to lateral capillary forces that cause floating pollen to come together to form pollen rafts and transports pollen rafts tangentially on a water surface toward a depression in the water surface created by a stigma. We, therefore, wanted to study how the presence of a trace amount of surfactant in the water influences the movement of pollen. We added different concentrations of Dawn dishwashing liquid surfactant (measured in ppm) to 500 ml of water to find out the optimal concentration required to disrupt the pollen transport process. We considered concentrations ranging from 2 ppb (parts per billion) to 200 ppm (parts per million). The surface tension of water decreased with increasing surfactant concentration; it was 72.417 dyn/cm for the native water, 71.22 dyn/cm for 2 ppb and 27.21 dyn/cm for 200 ppm. The presence of surfactant for this concentration range did not adversely influence the plants, at least not visibly. The leaves remained green and the anthers matured normally. However, there was a critical concentration above which the transport of pollen was affected, and there was a higher concentration at which the transport was completely disrupted. For concentrations below the critical value there was no noticeable effect.

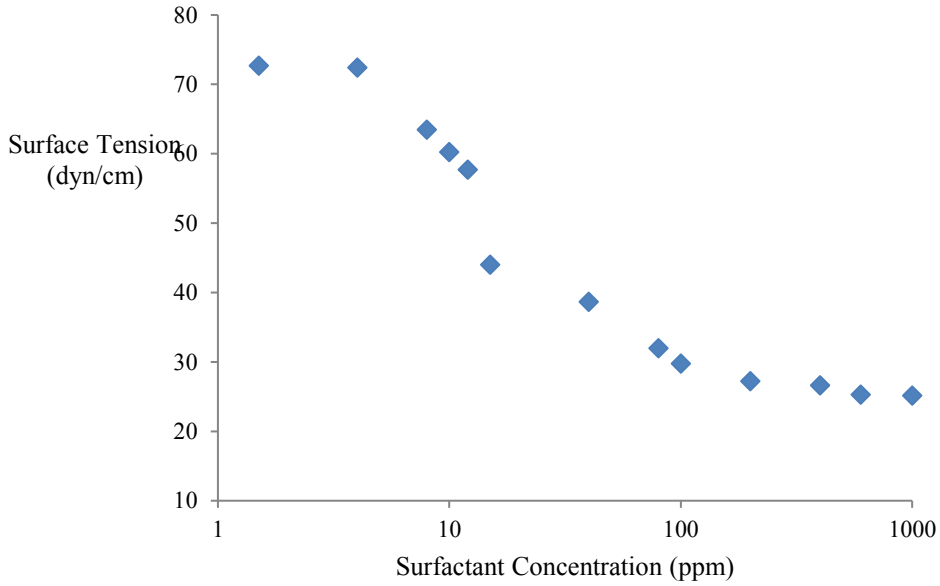

Figure 3.14 The surface tension of the native water as a function of the surfactant concentration.

The stems containing anthers were placed above and below the surface of surfactant mixed native water and the motion of pollen masses was recorded using the cameras mounted at the sides and above the water surface as was done for the native water cases (see Figure 3.5). We visually observed any changes in the pollen behavior to determine the critical surfactant concentrations at which the transport mechanisms were affected by the presence of surfactant.

3.4.1 Anthers in Native Water with 15 Ppm Surfactant

As discussed above, the pollen transport process was not affected when the surfactant concentration was between 2 ppb and 15 ppm. However, when the concentration was increased to 15 ppm, the behavior of pollen masses during the adsorption and dispersion phases was noticeably different. The anthers placed above the water surface opened up and the pollen masses detached from them normally, but most of the pollen masses did not partially disperse when they were adsorbed at the water surface (see Figure 3.15). For

the case where the anthers were placed below the water surface, the anthers dehisced their pollen masses into gas bubbles that carried them to the water surface. Some of the pollen masses dispersed partially after reaching the surface and some did not disperse and retained their kidney-like shape (see Figure 3.16). The behavior of pollen masses released below or above the water surface was similar. In both cases, pollen masses maintained their kidney-like shape with a smooth boundary. These floating pollen masses formed pollen rafts like they do on the native water and floated for several minutes. However, after a few minutes these undispersed pollen sedimented to the bottom. This indicates that the contact angle was reduced due to the presence of surfactant and so the contact line advanced on the surface of pollen mass completely covering the surface causing it to sink. Also, as pollen mass is denser than water, the vertical capillary force is required to keep it afloat, but its magnitude was reduced because pollen masses did not disperse and the surface tension was diminished due to the presence of the surfactant (see Figure 3.15c). At 15 ppm surfactant concentration, the surface tension was reduced to 44.02 dyn/cm from 72.42 dyn/cm for native water. The reduced surface tension prevented pollen masses (both those falling from the air and those rising from below) from dispersing and efficiently floating on the water surface.

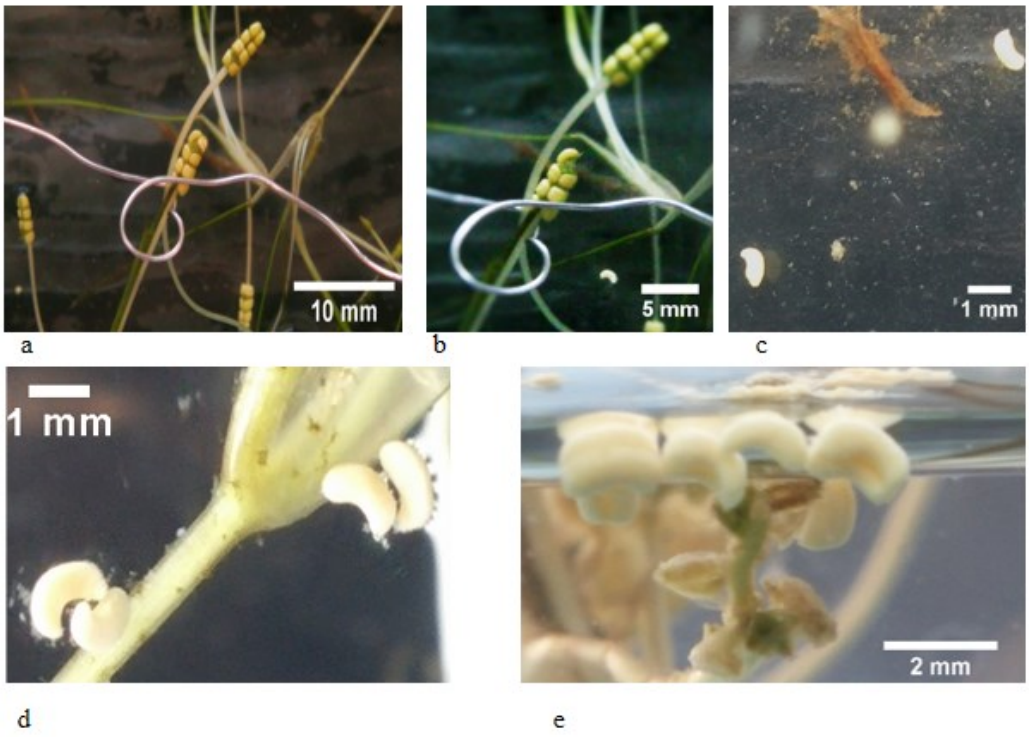

Figure 3.15 (a) Anthers placed above and below in native water mixed with 15 ppm surfactant (b)-(e) show the anther sacs falling from air onto water surface mixed with 15 ppm surfactant. (f)-(g) show the anther sacs raising to the top of water surface from below and due to the presence of surfactant the pollen masses are partially dispersed and few of them did not disperse.

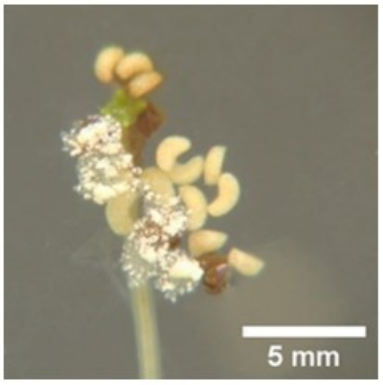

Figure 3.16 The figure shows that at 15 ppm only a fraction of the pollen masses that rose to the surface with the help of gas bubbles dispersed. Both dispersed and undispersed pollen masses clustered together under the action of lateral capillary forces. However, after a few minutes most of them sedimented to the bottom.

3.4.2 Anthers in Native Water with 100 ppm Surfactant

We next describe the case for which the concentration of surfactant in the native water was 100 ppm. At this concentration, the surface tension was reduced to 29.74 dyn/cm from 72.42 dyn/cm for native water. As for the unadulterated native water, when the anthers opened up they released gas bubbles to transport their pollen masses to the water surface and for the anthers placed above the water surface pollen simply fell on to the surface. The presence of surfactant, however, diminished the tendency of pollen grains to breakup from the pollen mass to adsorb onto the surface of the bubble (see Figure 3.17). The pollen mass remained intact and maintained a kidney-like shape. The gas bubbles caused the pollen masses to detach from the anthers, but they were not always carried to the water surface. In most cases, instead of rising up with the bubble to the water surface, the pollen masses detached from the bubble and sedimented to the bottom of the beaker. The pollen masses maintained their kidney-like shape, indicating that they remained intact during this process (see Figure 3.17b). The anther sac also sedimented to the bottom of the beaker.

In some cases, the pollen mass did rise to the water surface along with the gas bubble, but did not disperse even after having been adsorbed at the water surface where it maintained its kidney-like shape (see Figure 3.18b). It floated on the surface for several minutes, but eventually desorbed as the contact line moved to cover the surface with water. In addition, the vertical capillary force was smaller because the pollen mass did not disperse after reaching the water surface and so the boundary length over which the surface tension acted was smaller, and the surface tension was smaller due to the presence of surfactant.

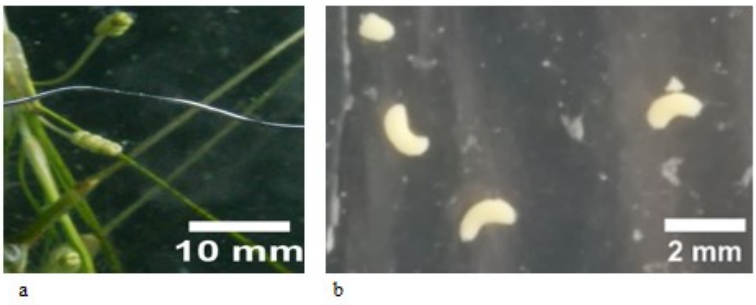

Figure 3.17 Pollen mass released below the surface in water which contained 100 ppm of surfactant. (a) Anther pods (b) Undispersed anther sacs at the bottom of the beaker.

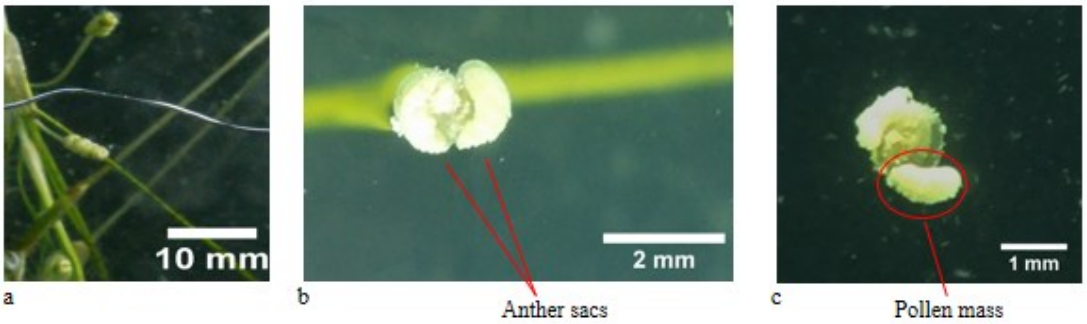

Figure 3.18 The pollen mass rose to the water surface along with the bubble, but it did not disperse and eventually sedimented to the bottom of the beaker. (a) Anther pods (b) Anther sacs in kidney like shape on water surface (c) After several minutes the undispersed pollen mass at the bottom of the beaker.

As in unadulterated native water, when anthers placed a few millimeters above the surface of native water with 100 ppm surfactant concentration matured, the pollen mass detached and fell on to the water surface. The presence of surfactant did not alter the maturation process (see Figure 3.19). The pollen mass remained essentially clumped, but some small pieces broke away from the main mass which was also the case in native water (see Figure 3.10). The pollen mass dispersed immediately after coming in contact with the water surface, but the larger sized pollen clumps were not trapped at the water surface. The fraction of the pollen trapped at the water surface was significantly smaller

than on native water and 15 ppm surfactant water as only individual pollen grains and small pollen clumps were trapped. This, as discussed above, was a consequence of the fact that the presence of surfactant reduced the surface tension and the contact angle. The latter caused the contact line to advance and cover the pollen surface with water. The vertical capillary force was reduced also because of a reduced tendency of pollen masses to disperse. Thus, the trapped layer was essentially a monolayer of individual pollen grains and small clumps.

These dispersed pollen monolayers did not combine to form a raft and the air currents caused them to move around on the surface (see Figure 3.19e). This is indicative of the fact that the buoyant weight of pollen monolayers was too small and it did not cause significant surface depression. On native water, on the other hand, the pollen partially dispersed into densely packed clusters that combined to form pollen rafts.

Figure 3.19 Adsorption of pollen from anther pods placed above the surface of water containing 100 ppm surfactant. (a) Anther pods above water surface, (b) A pollen mass falling onto the water surface, (c) Pollen spreading into a monolayer, (d) A portion of the pollen sedimenting, and (e) Monolayers moving around on the water surface but do not combine.

To understand this further we studied the dispersion of pollen clumps under a microscope by dropping them on to the surface of native water with 100 ppm surfactant concentration in a petri dish. The pollen clumps in this experiment were the pollen masses that were captured on a microscope slide as they fell from the anthers. When a pollen clump was dropped on to the surface of water only a relatively small portion consisting of a monolayer of individual grains and small clumps was adsorbed trapped on the water surface (see Figure 3.20).

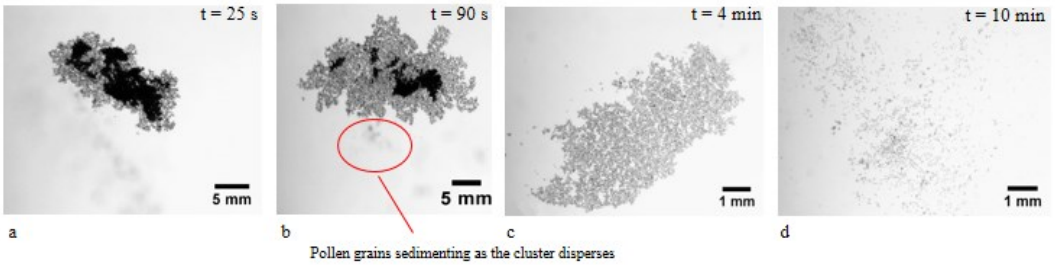

Figure 3.20 Dispersion of pollen clumps on the surface of native water with 100 ppm surfactant concentration observed under microscope. (a) The pollen clump started to disperse immediately. (b) The pollen clump completely dispersed and a large part of it sedimented. (c) Monolayer of individual pollen grains and small clusters remaining on the water surface. (d) A large portion of the pollen sedimented.

To summarize, the presence of surfactant reduces surface tension and contact angle of water which adversely affect the pollination mechanisms. For example, when the surfactant concentration is 100 ppm the surface tension is reduced to 29.74 dyn/cm which reduces the maximum possible vertical capillary force that can act of a pollen mass, and the reduction in the contact angle causes pollen grains to become covered with water and thus sink. This combined with the fact that pollen masses do not disperse caused most of the pollen mass not to get trapped at the surface and so it was not available for pollination.

3.5 Discussion and Conclusions

We observed two mechanisms by which the pollen released from male inflorescences of *Ruppia maritima* is adsorbed on a water surface: 1) inflorescences rise above the water surface and after they mature their pollen mass falls onto the surface as clumps and disperses as it comes in contact with the surface; 2) inflorescences remain below the surface and produce gas bubbles which carry pollen mass to the surface where it disperses. In the second case, some pollen grains were also released onto the bubble surfaces before they detached from the inflorescences. These pollen grains adsorbed on the bubble surfaces were also carried to the water surface and were concentrated in the lower portion of the bubble which was below the water surface. The video recordings show that often the pollen mass within a bubble remained undispersed for several minutes and then suddenly the bubble burst causing the dispersion of the pollen onto the water surface. The mechanism by which the bubble burst at the surface and the encapsulated pollen mass dispersed on to the water surface is not clear from the video recordings.

In both cases, the pollen mass partially dispersed with a densely packed region of pollen grains in the middle which was surrounded by a monolayer of pollen grains. The latter appeared translucent compared to the densely packed region because it contained mostly a single layer of grains with some smaller clumps within. The process by which a pollen mass disperses is qualitatively similar to the process by which a clump of powder disperses on a water surface. The dispersed area of a pollen mass released above the water surface was smaller than that of a pollen mass released below the water surface. However, in both cases dispersed pollen masses floated and combined with others to

form pollen rafts. It is not known which of these pollen rafts were more efficient for pollination.

Clustering driven by lateral capillary forces is essential for efficient hydrophily for two reasons. First, it causes floating pollen masses to come together to form pollen rafts. Second, pollen rafts deform the water surface substantially more than a single pollen grain because of their larger size and buoyant weight, and therefore, they are more strongly attracted to the depressions created by the stigmas (see Figure 3.14). Since the attractive capillary force on a pollen raft toward a stigma is much larger than on a single pollen grain, the former is more likely to reach the stigma which increases the probability of pollination. For this reason, the pollen rafts are also referred to as the search vehicles.

We also observed that the attraction between individual pollen grains, and also between monolayers that did not have the inner dense pollen cores, was weak, and therefore they clustered very slowly or simply moved around on the surface because of the water currents without clustering. The capillary force between two floating particles varies as the product of their buoyant weights, and so the magnitude of the force varies as the second power of the density difference and the third power of the product of their radii. The density mismatch for the pollen grains was small as their density was only slightly larger than the water density and their size was about 40 μm. The capillary force between pollen grains was comparable to the Brownian force and so was not large enough to cause them to cluster[5, 6]. This was also the case for the monolayers of pollen grains. Therefore, lateral capillary forces can efficiently transport pollen toward the depressions created by the stigmas when the buoyant weight of search vehicles is

sufficiently large and this can happen only when they consist of partially clumped regions.

Our observational data also shows that individual pollen grains of *Ruppia maritima* are attracted to each other by some as of yet unknown forces, suggesting that additional forces are important in the dispersion of these pollen grains. These cohesive forces between pollen grains are responsible for keeping the core of the dispersed clumps densely packed, which as we have discussed above, is important in the formation of pollen rafts and their transport toward a stigma. If these cohesive forces were not present, the pollen from an anther would disperse completely into a monolayer. This would decrease lateral capillary forces and thus the probability of pollination would also decrease. We also studied the dependence of the pollen transport process described above on the surface tension by adding a small amount of surfactant to the water which reduced the surface tension. The presence of surfactant interfered with the process of pollen transport. For anthers below the water surface, unlike before, most of the pollen masses were not transported to the surface by the bubbles. The reduced capillary force was not large enough to keep them attached to their bubbles as they raised to the surface and so they sedimented to the bottom without reaching the water surface.

Some pollen masses were transported to the water surface, but they did not disperse and after remaining on the water surface for a few minutes they also sedimented. The reduced surface tension was not large enough to keep the pollen masses afloat or to disperse them. For pollen masses released above the water surface, most of the pollen was not trapped at the surface, especially the larger sized clumps. The pollen that was adsorbed formed a monolayer which was not dense enough and so it was only weakly

attracted toward a depression in the water surface. We may, therefore, conclude that the presence of a small amount of surfactant can disrupt the surface pollination process in *Ruppia maritima.*

CHAPTER 4

CONCLUSIONS

Previous studies [4, 5] have shown that when a particle comes in contact with a liquid surface it is pulled into the interface towards its equilibrium height by the vertical capillary force and that during this process the particle can accelerate to a relatively large velocity normal to the interface. For example, a particle of radius 100 μm sprinkled onto the water surface may attain a velocity of the order of 1 m/s. It is also shown that a particle being adsorbed oscillates about its equilibrium height before coming to rest under viscous drag. These oscillations of the particle cause the fluid around it to move away.

The flow during particle adsorption at a fluid-liquid interface is studied in this work. During adsorption, the vertical capillary force pulling the particle into the interface gives rise to a transient streaming flow. This lateral streaming flow is studied using the Particle Image Velocimetry (PIV) technique. This flow is directed away from the test particle at the interface and below the interface this flow is directed towards the test particle. The PIV technique was used to study this flow for test particles of various sizes ranging from 550 μ to 2 mm. The test particles used were hollow glass spheres. The test particles were dropped in a petri dish containing DI water seeded with tracer particles which in the laser plane were illuminated by a green laser, and the flow of those partices was recorded by a camera and then analyzed with the help of a Matlab based PIV program.

The flow created due to adsorption was studied, and it was observed that even though the water near the test particle started to move as soon as the particle came in

contact with the surface, the adsorption-induced streaming flow intensity developed over a period of time. The temporal evolution of the flow was analyzed and plotted at different time intervals.

The intensity reached a maximal strength after a fraction of a second and then it decreased. For a 650 μm glass sphere the maximum flow strength occurred about 0.4 s after the particle come in contact, and for a 2 mm sphere after about 1.5 s. We also considered 1.1 mm, 0.85 mm and 0.55 mm glass spheres for which the maximal flow strength occurred after 0.75 s, 0.47s and 0.18 s, respectively. These results show that the time interval after which the maximal flow strength occurred decreased with decreasing particle size.

Flow created due to adsorption of two or more particles was also studied. When two or more particles are dropped simultaneously onto the surface their motion in the direction normal to the interface (and to the line joining their centers) gives rise to the strong repulsive hydrodynamic forces which cause them to move apart. This can be understood as a cumulative effect of each of the particles creating a streaming flow upon adsorption which drives the adjacent particle away. The velocity with which particles move apart increases with increasing number of particles. Results for 2-650 μm glass particles and nearly 10-30 650 μm glass particles are presented. Also, smaller sized particles disperse more readily because the importance of interfacial forces increases with decreasing particle radius.

A study of the mechanism of pollination in aquatic plant Ruppia maritima has also been presented here. This aquatic plant is native to brackish water conditions. Detailed results of anthers releasing pollen under different circumstances and the

migration of pollen towards stigma on the water surface are discussed. Due to the changing water levels affected by the tides (high or low), the anthers of the plant (sometimes the entire plant) are either submerged or above the water surface (see Figure 3.2). The stigma positions itself at the top of the water surface, creating a depression at its tip. We collected the plants along with the native brackish water that they grow in, and transported them back to our lab for experimental study. During experiments, the plants were placed in beakers (with native water) such that the anthers were above and below the water level. The process of anthers releasing pollen was recorded at 60 fps using cameras to understand the mechanism of pollen releasing from anthers and their transport towards the stigma. The size and shape of the pollen, anthers and stigmas are presented.

The studies reveal that, during high tide-when the anthers are submerged below the water surface, upon dehiscence the anthers release a gas bubble which carries the pollen mass to the water surface This is important because, in general, the pollen are denser than water and in the absence of a gas bubble the released pollen would not reach the water surface and would sink and cannot reach stigma. During low tide, when the anthers are above the water surface, the pollen released from the anthers reaches the water surface due to gravity.

The released pollen mass disperses on the water surface, which is similar to the particle dispersion discussed above. It is observed that the time taken for the pollen mass to disperse is different for different cases, when the pollen is engulfed in gas bubble. Results show that the pollen mass trapped in the gas bubble may disperse instantly upon reaching the water surface, or may take a few minutes to a few hours to disperse. Several of these dispersed pollen masses from same/different anthers come together to form a

pollen raft, which acts as a search vehicle on the water surface, moving in search of stigma. The pollen raft has a high probability of pollination compared to a monolayer of pollen or individual pollen floating on the water surface. This is because the lateral capillary attraction between a pollen raft and the stigma is stronger.

Surface tension plays a crucial role in the whole process of pollination. The vertical capillary forces help the dispersed pollen mass to stay afloat and the lateral capillary forces help in the formation of pollen rafts to reach the stigma. The influence of surfactant on the pollen dispersal mechanism is also studied and reported, as the surfactant can reduce the surface tension. This we established by adding dishwashing liquid surfactant to the native water in varying concentrations from 2 ppb to 200 ppm, to determine the optimum level of surfactant that can impact the mechanism.

The surface tension reduced from 72.41 dyn/cm for native water to 29.74 dyn/cm in water with 100 ppm surfactant concentration. The pollination mechanism was affected for concentrations of 15 ppm and above. At 15 ppm, it was partly affected, such that few of the released pollen did not disperse at the water surface and eventually sedimented, and few pollen masses dispersed and managed to form pollen rafts. At 100 ppm concentration, none of the released pollen masses dispersed and all sedimented to the bottom of the beaker. When pollen was released from anthers located above the water surface, the pollen dispersed completely into a monolayer and during this dispersion process a major portion of the pollen from the pollen mass was seen to be sedimenting to the bottom.

To study the role of salinity of native water in the whole process of pollination, pollen masses were released on the surface of pure water and were observed under

microscope to understand the dispersal behavior. The pollen mass dispersed completely into monolayer on the surface of pure water, whereas the pollen mass dispersed partially on native water.

APPENDIX A

VERTICAL FORCE BALANCE AND LATERAL CAPILLARY FORCES ON FLOATING POLLEN CLUSTERS

The pollen to ovule ratio in *Ruppia* and other seagrasses is relatively smaller, and so they have evolved efficient two-dimensional mechanisms for transporting their pollen [33]. As discussed in chapter 3, in *Ruppia maritima,* the pollen mass released below the water surface is carried to the surface by gas bubbles released by the anthers, and the pollen mass released above the water surface simply falls onto the surface. Once adsorbed at the air-water interface it can continue to float at the surface and travel laterally (tangentially) on the surface in search of a stigma. However, since *Ruppia* pollen mass is denser than water (density ~ 1.024 g/cm^3), if it is not adsorbed at the water surface it quickly sediments to the bottom.

In this appendix, we estimate the lateral and vertical capillary forces acting on the pollen grains and clusters trapped at a water surface that arise because of the deformation of the water surface that they cause. The vertical capillary force allows particles to float even though they are denser than water and the lateral capillary force causes them to move laterally. However, since the magnitude of lateral capillary force decreases with decreasing cluster size, there is a critical size below which the capillary force becomes negligible in the sense that the force is smaller than the Brownian force.

For simplicity, in our analysis we will assume that the pollen grains and clusters are approximately spherical. For an air-water interface, the interfacial tension is $\gamma = 0.07$

N/m, the air density is $\rho_a = 1$ kg/m^3, and the water density is $\rho_L = 1000$ kg/m^3. The capillary force $\boldsymbol{F_c}$ acting on a floating spherical particle (pollen mass) is given by

$$\boldsymbol{F_c} = \oint_{\mathrm{CL}} \boldsymbol{\gamma}\, ds = \gamma s_{cl} \sin\beta\, \mathbf{j} \tag{A.1}$$

The integral is along the contact line (CL), $\boldsymbol{\gamma}$ is the surface tension acting at the contact line, **j** is the unit vector normal to the surface, $\gamma \sin\beta$ is the vertical component of surface tension, β is the angle the contact line makes with the surface, s_{cl} is the perimeter of contact line along which the surface tension acts, and γ is the magnitude of $\boldsymbol{\gamma}$. In general, the force has both horizontal and vertical components, but because of the symmetry, the force on an isolated spherical particle is in the vertical direction. The vertical capillary force is maximum when the surface tension acts vertically along the contact line, and the maximum possible value is γs_{cl}. The maximum vertical force on a partially dispersed pollen mass is greater than that on an undispersed pollen mass because for the former the perimeter of contact line is longer.

Let us consider the vertical force balance for the i^{th} particle trapped in the water surface. The buoyant weight F_{bi} of the ith particle is balanced by the capillary force F_{ci},

$$F_{\mathrm{ci}} + F_{\mathrm{bi}} = 0. \tag{A.2}$$

The buoyant weight can be written as $F_{bi} = -g\rho_L a_i^3 f_{bi}(\frac{\rho_a}{\rho_L}, \frac{\rho_{pi}}{\rho_L}, \theta_{ci}, \frac{h_{2i}}{a_i})$, where g is the acceleration due to gravity, ρ_{pi} is the density of the i^{th} particle, θ_{ci} and h_{2i} define the

floating position for the i^{th} particle (see Figure. A.1), and f_{bi} is the dimensionless buoyant weight which is a function of the included arguments (see [15]).

It is easy to deduce from Fig. A1 that the capillary force F_{ci} can be written as $F_{ci} = -2\pi\gamma a_i \sin\theta_{ci} \sin\left(\theta_{ci} + \alpha_i\right)$, where α_i is the three-phase contact angle on the surface of the i^{th} particle (see [4] for the details). Using these expressions in equation (A.1), we obtain

$$F_{ci} = -2\pi\gamma a_i \sin\theta_{ci} \sin\left(\theta_{ci} + \alpha_i\right) = -F_{bi}$$

$$= g\rho_L a_i^3 f_{bi}\left(\frac{\rho_a}{\rho_L}, \frac{\rho_{pi}}{\rho_L}, \theta_{ci}, \frac{h_{2i}}{a_i}\right) \qquad \text{(A.3)}$$

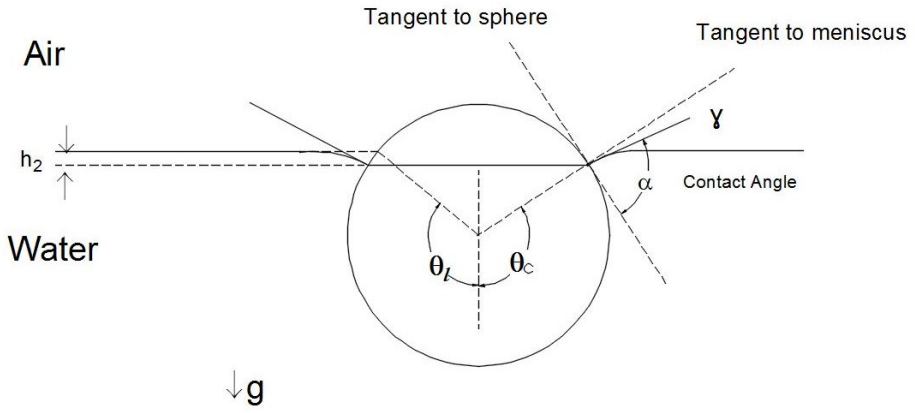

Figure A.1 Schematic of a sphere of radius *a* hanging on the contact line at θ_c. The point of extension of the flat meniscus on the sphere determines the angle θ_l and height h_2. The contact angle α is fixed by the Young-Dupré law and angle θ_c by the force balance.

The equation A.3 takes the following dimensionless form

$$2\pi \sin\theta_{ci} \sin(\theta_{ci} + \alpha_i) = -\mathrm{B}\ f_{bi}\left(\frac{\rho_a}{\rho_L}, \frac{\rho_{pi}}{\rho_L}, \theta_{ci}, \frac{h_{2i}}{a_i}\right) \tag{A.4}$$

where $\mathrm{B} = \rho_L a_i^2 g/\gamma$ is the Bond number. For a pollen grain of 40 μm diameter, B = $5\text{x}10^{-5}$ and for a pollen clump of 1 mm diameter, B = 0.035. Thus, the Bond number for pollen clusters smaller than one millimeter is much smaller than one. When the Bond number is small the interfacial deformation is small, and the position of the particle in the interface is determined primarily by the contact angle. Such small clusters therefore can float on the surface without sinking. However, the presence of surfactant decreases interfacial tension and the contact angle, which, as discussed in chapter 3, can cause pollen clusters to sink.

The external vertical force acting on a particle in equilibrium is balanced by the vertical component of capillary force that arises because of the deformation of interface. The profile of the deformed interface around a particle can be obtained by integrating Laplace's equation and using as boundary conditions that the interface far away from the particle is flat and that the angle between the interface and the horizontal at the particle surface is known in terms of the total external force acting on the particle. It can be shown that the interface height $\eta_i(r)$ at a distance r from particle i is given by (see [1, 15])

$$\eta_i(r) = a_i \sin(\theta_{ci}) \sin(\theta_{ci} + \alpha_i) K_0(qr) \tag{A.5}$$

where $K_0(qr)$ is the modified Bessel function of zeroth order and $q = \sqrt{\frac{(\rho_L - \rho_a)g}{\gamma}}$.

Now, let us consider a second particle *j* at a distance *r* from the first particle. The height of the second particle is lower because of the interfacial deformation caused by the first particle, and thus the work done by the gravity (buoyant weight) on particle *j* is

$$W = -\eta_i(r)\, w_j, \tag{A.6}$$

where $w_j = F_{bj}$ is the vertical force acting on the j^{th} particle.

Using equations (A.3) and (A.4), in equation (A.5) we obtain

$$W = -\frac{w_i\, w_j}{2\pi\gamma} K_0(qr)$$

$$= \left(\frac{4}{3}\pi a_i^3 \rho_p g f_{bi}\right)\left(\frac{4}{3}\pi a_j^3 \rho_p g f_{bj}\right)\frac{K_0(qr)}{2\pi\gamma} \tag{A.7}$$

In Figure A.2, $W/(kT)$ is plotted as a function of the particle radius for two identical particles in contact with each other ($r = 2a$), where *k* is the Boltzman constant and T = 300°K is the temperature. The parameter values are assumed to be $\rho_p = 1050$ kg/m^3, $a_1 = a_2 = a$, and $f_{b1} = f_{b2} = 0.5$. The figure shows that for these parameter values, $W/(kT) = \sim 1$ for a = 10.0 μm, $W/(kT) = \sim 50$ for a = 20 μm, and $W/(kT) = \sim 1000$ for a = 33 μm.

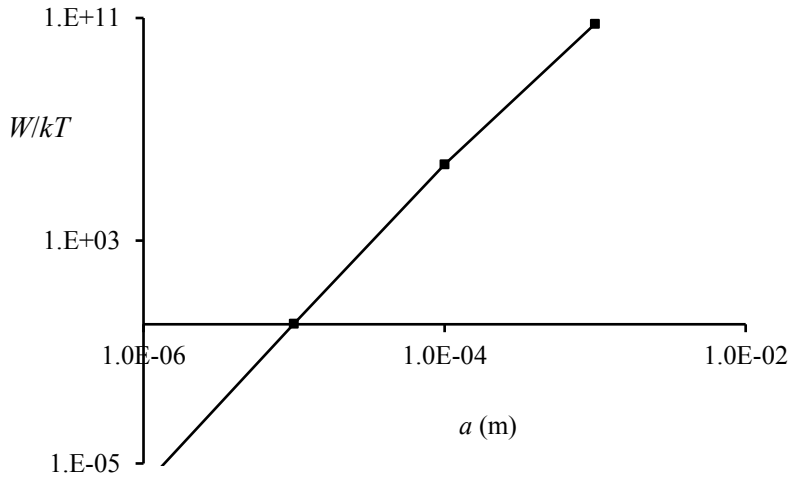

Figure A.2 The capillary attraction energy (W_c) divided by kT is plotted against the particle radius. The parameters are: $\gamma = 0.07$ N/m, $\rho_a = 1$ kg/m^3, $\rho_L = 1000$ kg/m^3, $\rho_p = 1024$ kg/m^3, $a_1 = a_1 = a$ and $r = 2a$.

Previous studies have shown that for particles suspended in a fluid to cluster under the action of attractive forces the associated interaction energy should be about a hundred times *k*T or larger. According to the above analysis the capillary interaction energy between two pollen grains of 40 μm diameter (a = ~20 μm) floating on a water surface is approximately of O(100*k*T) which is consistent with our experimental observation that individual pollen grains attract only weakly and so they do not cluster. For pollen clusters, on the other hand, the capillary interaction energy is orders of magnitudes larger, with the strength increasing with increasing cluster size. The capillary force between a single pollen grain and a cluster is also larger (again, depending on the cluster size) than that between two grains. These results are consistent with experiments which showed that partially dispersed pollen clusters combined together under the action of lateral capillary forces to form pollen rafts, but individual pollen grains, including their monolayers, did not cluster. The force was greater between a pollen raft and a stigma on

the water surface, as the latter caused the interface to deform much more significantly than did a pollen mass.

The lateral capillary force between particles *i* and *j* is given by

$$F_{lc} = -\frac{d\mathrm{W_c}}{dr} = -\frac{w_i\, w_j}{2\pi\gamma}\, qK_1(qr) \tag{A.8}$$

where $K_1(qr)$ is the modified Bessel function of first order. For two particles far away from each other, the above reduces to

$$F_{lc} = -\frac{w_i\, w_j}{2\pi\gamma}\frac{1}{r} = -\left(\frac{4}{3}\pi a_i^3 \rho_{pi} g\, f_{bi}\right)\left(\frac{4}{3}\pi a_j^3 \rho_{pj} g\, f_{bj}\right)\frac{1}{2\pi\gamma\, r} \tag{A.9}$$

The lateral capillary force depends on the product of the buoyant weights of the two particles.

Furthermore, Equations (A.6) and (A.8) also imply that with increasing distance between two particles the capillary interaction energy decays and the attractive force between them decreases. For example, the force between a 1 mm sized cluster and a stigma remains significant within a distance of ~ 1 cm from the stigma. However, the force between a raft of 5 mm radius and a stigma remains significant within a distance of ~10 cm. The size of a pollen raft depends on the number of pollen masses that combined to form the raft. For simplicity, it is assumed that the pollen rafts are homogenous and spherical even though the actual pollen rafts are pancake shaped consisting of partially

dispersed pollen masses which are held together by lateral capillary forces. The volume of pollen mass in a raft can be used find the radius of an equivalent spherical particle.

APPENDIX B

GOVERNING EQUATIONS AND NUMERICAL RESULTS

In this appendix, the results of our numerical study aimed at modeling the role of lateral capillary forces between a pollen raft and the stigmas in determining the probability that a pollen raft or cluster would reach a stigma are presented. Previous studies on modeling of pollen mechanisms in aquatic plants were based on a random-search theory and a biophysical model which considered the role of surface water velocity [88-89]. They did not consider the role of surface tension which plays an important role when pollination process occurs on water surface, as is the case in *Ruppia maritima*. In our model based on momentum conservation, we also consider the lateral capillary forces that act between a pollen raft and a stigma. The numerical study assumes that the pollen raft is already adsorbed on the water surface. As noted earlier in chapter 3, a pollen raft adsorbed on a water surface is constrained to remain on the surface, but can move laterally on the surface under the action of lateral forces.

The lateral capillary and hydrodynamic forces acting on a raft are computed based on the physical parameter values that correspond to *Ruppia* pollination. The former arises because of the deformations caused by the raft and the stigmas, and the latter due to the flow on surface water. The probability that a pollen raft will come in contact with a stigma depends on factors such as the size of the pollen raft, the magnitude and direction of surface water velocity, and the surface density of floating stigmas, i.e., their number per unit area of the water surface. In our simulations, we will assume that the stigmas are distributed uniformly on the surface in a rectangular periodic lattice and the direction of

surface flow is along a lattice direction. The stigmas are assumed to be fixed at their locations. This is a reasonable approximation as the plants are rooted and so they do not migrate because of the water flow. However, since the pollen stems are flexible, stigmas can oscillate about their equilibrium positions. The lattice size is assumed to be finite in the flow direction and periodic in the direction normal to the flow direction (see Figure B.1). The computational model allows us to evaluate the role of parameters in pollination.

To estimate the probability of capture (or the capture rate), a large number of pollen rafts were released (one at a time) at different upstream locations from the lattice of stigmas and their lateral upstream positions were varied to account for all possible trajectories (see Figure B.1). The capture rate is defined to be the fraction of rafts captured by the stigmas. A raft was assumed to be captured if it came in contact with a stigma, but if it left the lattice without coming in contact with any of the stigmas it was assumed that it was not captured. A raft and a stigma were assumed to be in contact if the distance between them was smaller or equal to the sum of their radii. Also, the surface water velocity and the size of pollen rafts were varied to study their influence on the capture rate.

Let us assume that there are n stigmas on the surface. The capillary force F_i between a pollen raft p, and the i^{th} stigma is given by:

$$F_{pi} = \frac{w_p\, w_i}{2\pi\gamma}\frac{1}{r} \tag{B.1}$$

Here w_p and w_i are respectively the buoyant weights of the pollen raft and the i^{th} stigma, γ is the interfacial tension, and r is the distance between them. As described in the Supplementary Information of [6], $w_p = \left(\frac{4}{3}\pi a_p^3 \rho g f_p\right)$ and $w_i = \left(\frac{4}{3}\pi a_i^3 \rho g f_i\right)$, where a_p and a_i are the effective radii of pollen and stigma respectively, ρ is water density, and f_p and f_i are dimensionless buoyant weight of the raft and stigma respectively. The size of a stigma in this study is taken to be the average size (diameter 3.0 mm) and the density is assumed to be the same as the pollen density 1.024 g/cm^3. Notice that the capillary force decreases with increasing r, and therefore the pollen raft is attracted more strongly by a stigma that is closer. In our simulations $\mu = 0.89\ cP, \gamma = 0.072\ N/m$. The size of pollen rafts was varied. The values of the remaining parameters were estimated to be $f_p = 0.5$, $f_i = 1.0$, and $\xi = 0.5$. The number of stigmas n in our simulation was held fixed at 120.

The total capillary force acting on the pollen raft due to the stigmas can be obtained by a pair-wise summation of the individual interaction forces, which gives

$$\mathbf{F}_p = \sum_{i=1}^{n}\left(-\frac{w_p\, w_i}{2\pi\gamma}\frac{\mathbf{e}_{ip}}{r_{ip}}\right). \tag{B.2}$$

Here $\mathbf{e}_{ip}$ is the unit vector from the center of stigma i to the center of pollen raft p and r_{ip} is the distance between them.

When the velocity of the pollen raft differs from the local surface water velocity at its center, it also experiences a drag force. The raft velocity relative to the local water velocity remains small because of its small size, and so we can use the Stokes equation to estimate the drag

$$\mathbf{F}_{dp} = -6\pi\mu\varsigma a_p(\mathbf{u}_p - u_w\mathbf{j}), \tag{B.3}$$

where $\mathbf{u}_p$ is the raft velocity, $u_w\mathbf{j}$ is the velocity of water at the surface which is assumed to be in the y-direction, μ is the water viscosity and ς is a correction parameter which accounts for the fact that the pollen raft is partially immersed in the water.

The momentum equation governing the motion of a pollen raft is obtained by equating the rate of change of momentum to the sum of forces acting on the raft (given by Equations (B.2) and (B.3)), which gives

$$m_p \frac{d\mathbf{u}_p}{dt} = \sum_{i=1}^{n}\left(-\frac{w_p\, w_i}{2\pi\gamma}\frac{\mathbf{e}_{ip}}{r_{ip}}\right) - 6\pi\mu\varsigma a_p(\mathbf{u}_p - u_w\mathbf{j}) \tag{B.4}$$

where m_p is the effective mass of the pollen raft.

Equation (B.4) implies that when the drag force is much larger than the capillary force, the trajectory of the pollen raft would be the same as that of a material element of water on the surface. In this case, which occurs when u_w is relatively large, only those rafts that directly collide with a stigma would be captured. On the other hand, when u_w is negligibly small or zero the capillary force determines the raft's trajectory, and since the

capillary force is directed toward a stigma, the raft would be captured in this case. When the velocity is between these two limiting values the probability of capture depends on u_w as well as on the raft's trajectory. Notice that since the capillary force decays with the distance, only those rafts whose trajectory brings them sufficiently close to a stigma would be captured. Also, when u_w is larger, a raft would be captured only if it is on a trajectory that brings it closer to the stigma.

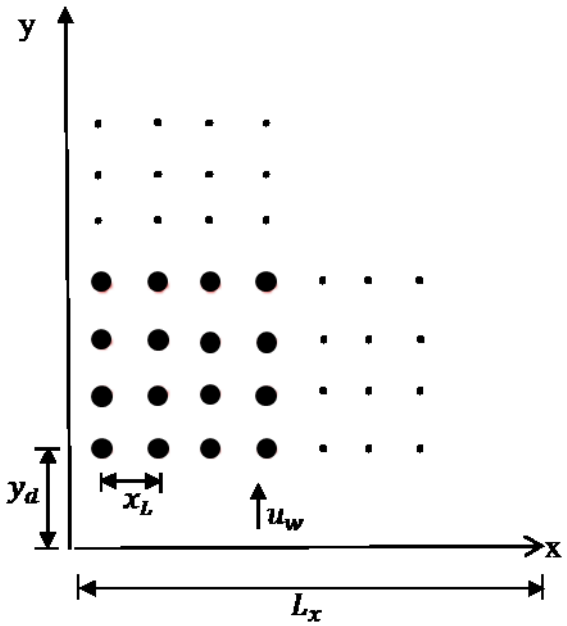

Figure B.1 Rectangular lattice of stigmas on a water surface. The initial lateral upstream locations (x) of the pollen rafts were varied to sample the possible trajectories.

An estimate of the critical water velocity on the surface for which the drag and capillary forces are equal can be obtained by assuming that there is only one stigma on the surface and equating the forces given by Eq. (B.1) and Eq. (B.3), which gives

$$u_{w,crit} = \frac{w_p\, w_i}{24\pi^2 \gamma \mu \varsigma a_p^2}. \tag{B.5}$$

In evaluating the above, we have assumed that the distance between the stigma and the pollen raft is two times the raft radius. This expression gives the critical velocity above which the pollen is unlikely to be captured. In figure B.2, the critical velocity is plotted as a function of the raft radius. The figure shows that as the raft radius increases, the critical velocity also increases. Also, for a given u_w there is a critical raft size such that the rafts smaller than this size are not likely to be captured (unless they collide directly with a stigma). However, also note that when more stigmas are present the capillary force is larger which increases the probability of capture, but this problem has to be investigated numerically, as we do below.

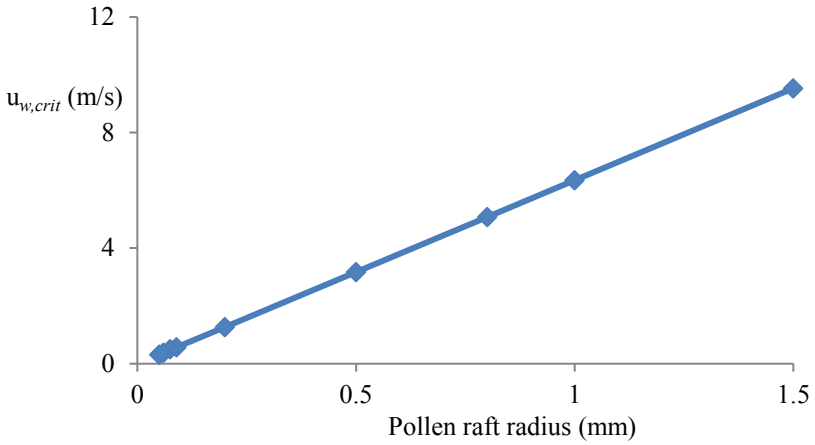

Figure B.2 The critical velocity of water on the surface for a stigma with radius $a_i = 0.002\,m$ is plotted as a function of pollen raft radius. Notice that the critical velocity increases with increasing raft radius which indicates that the capillary forces are stronger for larger rafts.

In our simulations, *n* stigmas were placed on a periodic lattice. Then, *m* pollen rafts were released one at a time from the upstream positions. The initial raft positions were uniformly distributed along the x-axis and were released at a fixed upstream distance from the lattice which was varied to study its role. The governing equations were numerically integrated in time to obtain the trajectories of pollen rafts. The system of

equations was discretized using an implicit second order scheme in time. The time step used in the simulations was selected by verifying that the simulation results did not change when the time step was reduced. A raft was either captured by a stigma or escaped from the lattice.

B.1 Simulation Results

We first present the results, which show that the numerically computed capture rate of the pollen rafts is independent of the time step used and of the number of rafts released when a sufficiently large number of rafts are released. Figure B.3 shows the percentage of pollen rafts captured for two different time steps as a function of the number of rafts released. The percentage of rafts captured did not change significantly when the time step was reduced by a factor of 10. The difference between the results for the two time steps diminished as the number of pollen rafts released was increased. Also, when about 1000 rafts were released the capture rate was already independent of the number of rafts released.

Figure B.4 shows that the capture rate is independent of the upstream distance y_d from the lattice at which the rafts are released. The same number of rafts were released and they were uniformly distributed along the x-direction. Thus, although the probability of capture of a raft in a given lattice of stigma depends on its trajectory, it is possible to define an average capture rate. The probability of capture of a raft released at an arbitrary upstream position can be approximated by the average capture rate. Also, the average capture rate can be used to quantify the roles of various parameters, as we do below.

We next study the dependence of capture rate on the distance between two stigmas (x_L) in the direction normal to flow, the surface water velocity u_w, and the size

of pollen rafts. The area fraction of stigmas, defined to be the number of stigmas per unit area of the water surface, is equal to $\frac{1}{x_L x_F}$, where x_F is the distance between the stigmas in the flow direction. For a fixed value of x_L, the area fraction is inversely proportional to x_L. Thus, the capture rate is expected to increase with decreasing x_L as there are more stigmas present per unit area.

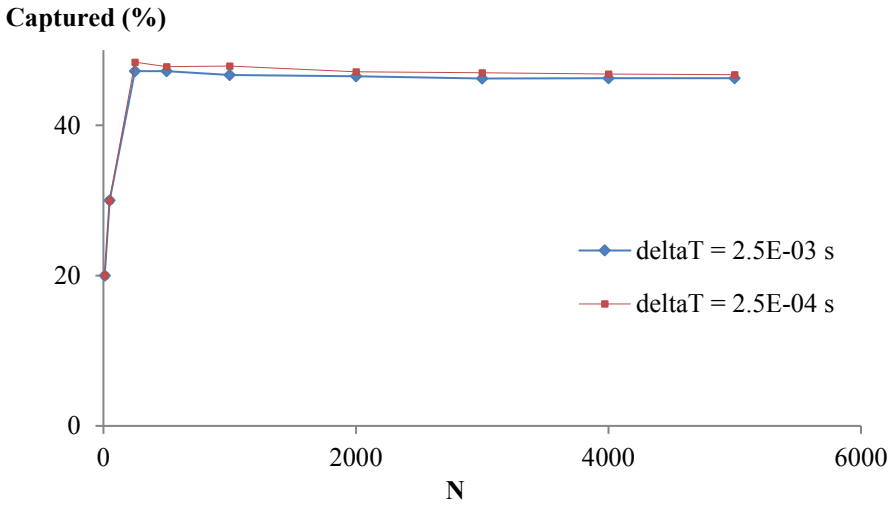

Figure B.3 The percentage of pollen rafts captured is shown as a function of the number of pollen rafts released (N) for two different time steps. The parameter values are: x_L = 0.5 m, y_d = 0.5 m, u_w = 0.3 m/s, a_p = 1 mm, and $a_i = 2\ mm$.

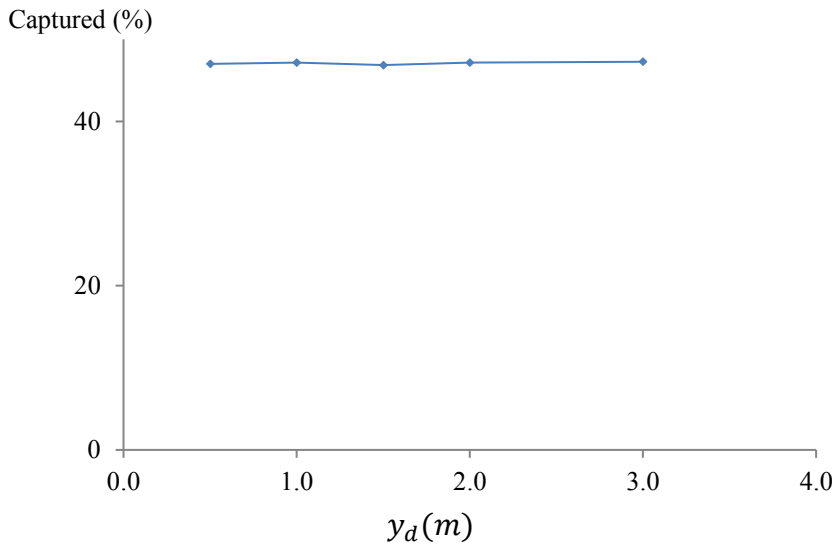

Figure B.4 The percentage of pollen rafts captured is shown as a function of the upstream distance from which the rafts were released. The parameters values are: x_L = 0.5 m, u_w = 0.3 *m/s*, a_p = 0.001 m,$a_i = 0.002\ m$ and N = 3000.

In Figure B.5, the capture rate is plotted as a function x_L for u_w = 0.3 m/s. As expected, the capture rate increases as x_L is reduced. The increase is due to two reasons. First, since the surface density of stigmas is greater, the average minimum distance between the pollen rafts trajectories and the stigmas is smaller. This increases the percentage of capture as the fraction of pollen rafts coming into contact with the stigmas is larger. The second reason is that the relative importance of capillary force increases with decreasing distance, since the capillary force increases with decreasing distance. Therefore, the attractive force between the pollen rafts and the stigmas is greater and so they are more likely to be captured. On the other hand, when the distance between the stigmas is larger the percentage of capture diminishes as only those rafts that come sufficiently close to a stigma are captured.

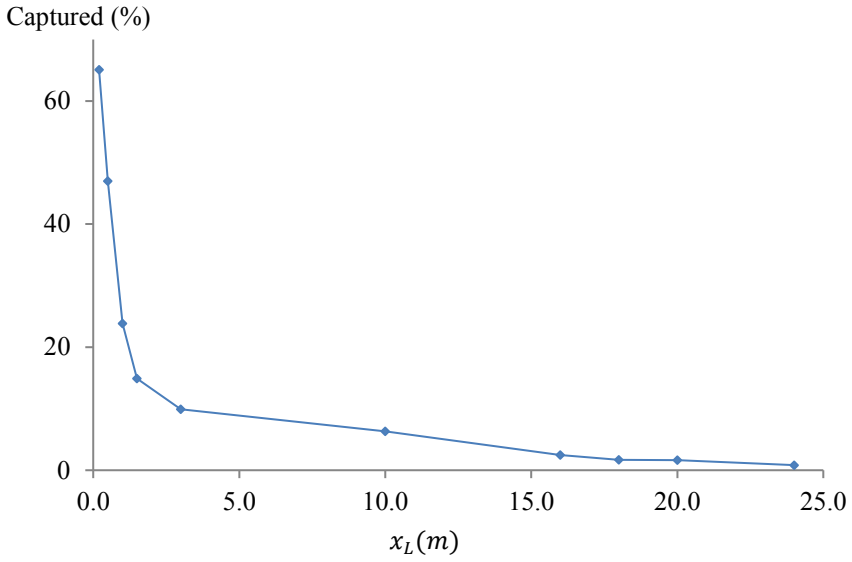

Figure B.5 The percentage of pollen rafts captured is shown as a function of x_L for u_w = 0.3 *m/s*, y_d = 0.5 *m*, a_p = 1 *mm*, $a_i = 2\ mm$, and N = 3000.

For raft radius between 50 μm and 1.5 mm, the effect of surface water velocity u_w on the capture percentage is shown in figure B.6a. The radius 50 μm is approximately 2.5 times the mean radius of a single pollen grain, and 1.5 mm is the average radius of pollen rafts. The capture rate is maximal for the smallest speed considered, i.e., 100 mm/s. In fact, at this speed, the capture rate is 100% for the rafts that have radius larger than 0.2 mm. This is because for them the capillary force is the dominant force and so all of the rafts released upstream of the stigma lattice are captured. The capture rate decreases from this maximal value when u_w is increased. The decrease is faster for the smaller rafts. For example, when u_w = 1 m/s and the raft radius is 1 mm, it decreases to 30%. For a 1 mm raft the capture rate decreases to about 10.2% when u_w is 10 m/s. This means that about 10% of the pollen mass in 1 mm pollen rafts is deposited at the stigmas, the remaining 90% is swept away by the flow. On the other hand, about 18% of the

pollen mass in 1.5 mm pollen rafts is deposited at the stigmas, and about 3% of the pollen mass in 0.5 mm pollen rafts is deposited at the stigmas. Also, notice that for a fixed value of u_w the capture rate increases with increasing raft size. This is because the capillary force increases with increasing raft size, and so larger rafts are more likely to be captured by stigmas. Thus, for small u_w, there is a critical raft radius above which all the rafts are captured. This analysis assumes that the surface minimums are created by stigmas alone.

It is noteworthy that the capture rate for 50 μm pollen rafts (diameter 100 μm, consisting of about 10 pollen grains) is around 0.67% even when the surface water velocity is very small. This value of the capture rate is approximately the fractional cross-sectional length of the surface that is occupied by the stigma in the direction perpendicular to the flow direction, which means that only those pollen rafts that directly collide with a stigma are captured. The fractional cross-sectional length determines the fraction of the streamlines that intersect a stigma. This is because a 50 μm raft simply moves in the direction of the surface flow since the capillary force acting on it is negligible. In our simulations, it is assumed that a pollen cluster is captured if it comes in contact with a stigma. However, in the real problem the pollen cluster will be captured only if the capillary force acting on it is larger than the drag force. On the other hand, if the drag force on the cluster is larger, it will not attach to the stigma, as the flow would cause it wash away from the stigma. Also, our analysis assumes that the attractive force causing the initial attachment of a pollen cluster with a stigma is the capillary force. This leaves out the possibility that some other presently unkown attractive force between a pollen cluster and a stigma exists.

In Figure B.6b similar results are shown for the case where the stigma radius was 1.5 mm and the dimensionless parameter f_b = 0.5. These values for the stigmas were varied to study the role of stigma size and buoyancy on the capture rate. Raft radius was varied between 50 μm and 1.5 mm and the water speed between 10 mm/s and 50 m/s. The results are similar except that the capture rate for a given u_w is reduced due to the reduction in stigma size and f_b, both of which reduced the capillary force. However, the capture rate increased to the value in Figure B.6a when u_w was smaller. In other words, the results for the two cases are similar except that the critical speed at which the transition occurred in Figure B.6b is smaller since the capillary forces are smaller. These results show that the capillary forces play an important role in Hydrophilous pollination.

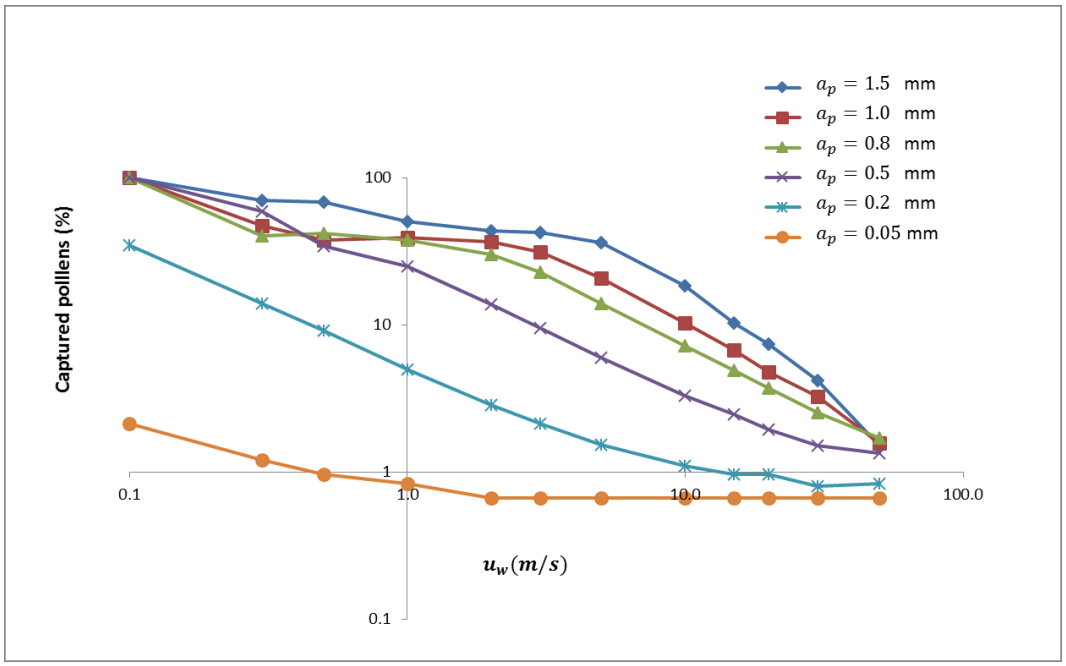

(a)

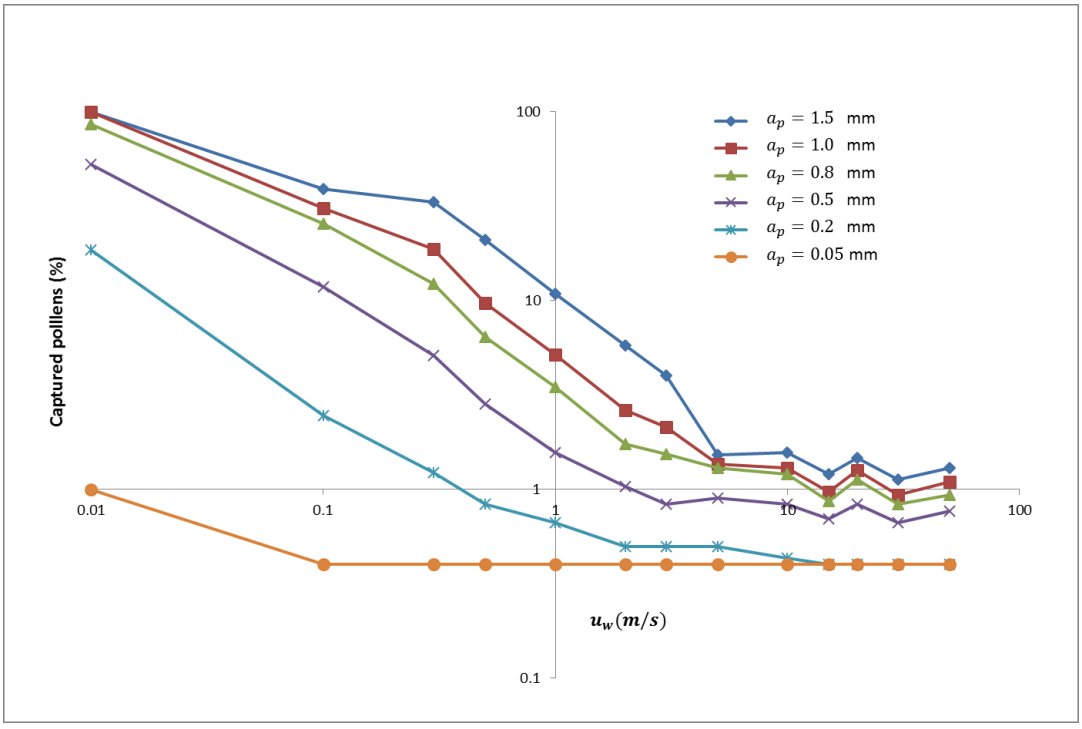

(b)

Figure B.6 The percentage of pollen rafts captured as a function of the surface water velocity u_w for six different raft sizes; x_L = 0.5 m and y_d = 0.5 *m*. *(a)* f_b = 0.9 and a_i = 2 *mm* and (b) f_b = 0.5 and a_i = 1.5 *mm*.

In summary, our numerical results imply that the probability of pollination increases when pollen grains combine to form rafts, since a higher percentage of the pollen mass is deposited at the surface minimums created by the stigmas. The increase happens for all surface water speeds, but it is most significant when the speed is between 0.1-10 m/s. The capture rate increases because the capillary force between a raft and a stigma increases with increasing raft size. The capture rate decreases with increasing u_w because the drag force causes the rafts to move in the direction of water flow reducing the influence of capillary force.

REFERENCES

1. Kralchevsky, P.A., et al. Capillary Meniscus Interactions Between Colloidal Particles Attached to a Liquid - Fluid Interface. Journal of Colloid and Interface Science, 1992. 151: p. 79-94.

2. Nicolson, M.M., The Interaction Between Floating Particles. Mathermatical Proceedings of Cambridge Philosophical Society., 1949. 45: p. 288.

3. Singh, P., D.D. Joseph, and N. Aubry, Dispersion and Attraction of Particles Floating on fluid-Liquid Surfaces. Soft Matter, 2010. 6: p. 4310-4325.

4. Gurupatham, S.K., et al. Particles Dispersion on Fluid-Liquid Interfaces. Particuology, 2011. 9: p. 1-13

5. Gurupatham, S.K., et al. Breakup of Particle Clumps on Liquid Surfaces. Powder Technology, 2012. 217: p. 288-297.

6. Singh, P., et al. Spontaneous Dispersion of Particles on Liquid Surfaces. Proceedings of the National Academy of Sciences, 2009. 106: p. 19761-19764

7. Aveyard, R., J.H. Clint, and T.S. Horozov, Aspects of the stabilization of emulsions by solid particles: Effects of line tension and monolayer curvature energy. Physical Chemistry Chemical Physics, 2003. 5: p. 2398-2409

8. Binks, B.P. and T.S. Horozov, Colloidal particles at liquid interfaces: An introduction. 2006: Cambridge University Press

9. Cox, P.A., Hydrophilous pollination. Annual Review of Ecology and Systematics, 1988. 19: p. 261-280.

10. Cox, P.A. and R.B. Knox, Two-dimensional pollination in hydrophilous plants: Convergent evolution in the genera Halodule (Cymodoceaceae), Halophila (Hydrocharitaceae), Ruppia (Ruppiaceae), and Lepilaena (Zannichelliaceae). American Journal of Botany, 1989. 176: p. 164-175

11. Dryfe, R.A.W., Modifying the liquid/liquid interface: pores, particles and deposition. Physical Chemistry Chemical Physics, 2006. 8: p. 1869–1883

12. Gust, D., T.A. Moore, and A.L. Moore, Mimicking Photosynthetic Solar Energy Transduction. Accounts of Chemical Research, 2001. 34: p. 40.

13. Pickering, S.U., Emulsions. Journal of the Chemical Society,London, 1907. 91(2): p. 2001.

14. Tang, Z., et al. Self-Assembly of CdTe Nanocrystals into Free-Floating Sheets. Science, 2006. 314: p. 274-278.

15. Wasielewski, M.R., Photoinduced Electron Transfer in Supramolecular Systems for Artificial Photosynthesis. Chemical Reviews, 1992. 92: p. 435.

16. Tsujii, K., Surface Activity: Principles, Phenomena, and Applications. 1998, Academic Press.

17. Fortes, M.A., Attraction and Repulsion of Floating Particles. Canadian Journal of Chemistry, 1982. 60: p. 2889.

18. Lucassen, J., Capillary Forces between Solid Particles in Fluid Interfaces. Colloids and Surfaces, 1992. 65: p. 131.

19. Aubry, N., et al. Assembly of Defect-Free Particle Monolayers with Dynamically Adjustable Lattice Spacing, in Proceedings of the National Academy of Sciences. 2008. p. 3711-3714

20. Bresme, F. and M. Oettel, Nanoparticle at Fluid Interfaces. Journal of Physics: Condensed Matter, 2007. 19(413101).

21. Singh, P. and D.D. Joseph, Fluid Dynamics of Floating Particles. Journal of Fluid Mechanics, 2005. 530: p. 31.

22. Stamou, D. and C. Duschl, Long-Range Attraction Between Colloidal Spheres at the Air-Water Interface: The Consequence of an Irregular Meniscus. Physical Review, 2000(62): p. 5263-5272

23. Nguyen, T.H., et al. An Analysis of the Thermodynamic Conditions for Solid Powder Particles Spreading Over Liquid Surface. Powder Technology, 2010. 201: p. 306-310.

24. Tüskea, Z., et al. The Role of the Surface Free Energy in the Selection of a Suitable Excipient in the Course of a Wet-Granulation Method. Powder Technology 2005. 155: p. 139–144

25. Zajic, L. and G. Buckton, The Use of Surface Energy Values to Predict Optimum Binder Selection for Granulations. International Journal of Pharmaceutics, 1990. 55: p. 155–164

26. Pillapakkam, S.B. and P. Singh, A Level Set Method for Computing Solutions to Viscoelastic Two-Phase Flow. Journal of Computational Physics, 2001. 174: p. 552-578.

27. Singh, P., T.I. Hesla, and D.D. Joseph, A Modified Distributed Lagrange Multiplier/Fictitious Domain Method for Particulate Flows with Collisions. International Journal of Multiphase Flows, 2003. 29: p. 495-509.

28. Singh, P., et al. The Role of Particle Inertia in Adsorption at Fluid-Liquid Interfaces. Physical Review 2011(83): p. 041606.

29. Currie, I.G., Fundamentals Mechanics of Fluids. 1974, New York: McGraw Hill.

30. Ackermann, J.D., Abiotic pollen and pollination: Ecological, Functional, and Evolutionary Perspectives In Pollen and Pollination. 2000: Springer Vienna.

31. Musunuri, N., et al. Transient Flow Induced by the Adsorption of Particles. Kona Powder and Particle, 2014. 31: p. 135-145.

32. Kendrick, G.A., et al. The Central Role of Dispersal in the Maintenance and Persistence of Seagrass Populations, BioScience, 2012, 62, pp.56-65

33. Philbrick, C.T. and Anderson, G.J., Implications of Pollen/Ovule Ratios and Pollen Size for Reproductive Biology of Potamogeton and Autogamy in Aquatic Angiosperms, Systematic Botany, 1987,12: 98:105.

34. Sculthorpe, Cyril. D., 1967, The Biology of Aquatic Vascular Plants, Edward Arnold, London.

35. Esau, K., 1977, Anatomy of Seed Plants. Second Edition, John Wiley and Sons, New York.

36. Den Hartog, C., & Kuo, J. (2007). Taxonomy and Biogeography of Seagrasses. In Seagrasses: Biology, Ecology and Conservation (pp. 1-23). Springer Netherlands.

37. Ito, Y., Ohi-Toma, T., Murata, J., & Tanaka, N. (2013). Comprehensive Phylogenetic Analyses of the Ruppia Maritima Complex Focusing on Taxa from the Mediterranean. Journal of plant research, 126(6), 753-762

38. Kantrud, Harold A. Wigeongrass (Ruppia maritima): A Literature Review. Fish and Wildlife Service Jamestown ND Northern Prairie Wildlife Research Center, 1991.

39. Hughes, A., et al. Associations of Concern: Declining Seagrasses and Threatened Dependent Species. Frontiers in Ecology and the Environment 7, no. 5 (2009): 242-246.

40. Short, Frederick T., et al. Natural and Human-Induced Disturbance of Seagrasses. Environmental Conservation 23, no. 1 (1996): 17-27.

41. Lehle, H. and Martin O., Importance of Boundary Conditions for Fluctuation-Induced Forces Between Colloids at Interfaces. Physical Review E75.1 (2007): 011602.

42. Galet, L., et al. The Wetting Behaviour and Dispersion Rate of Cocoa Powder in Water. Food and bioproducts processing 82.4 (2004): 298-303.

43. Planinšek, O., et al. The Utilization of Surface Free-Energy Parameters For The Selection of a Suitable Binder in Fluidized Bed Granulation. International journal of pharmaceutics 207.1 (2000): 77-88.

44. Eshtiaghi, N., et al. Liquid Marble Formation: Spreading Coefficients or Kinetic Energy? Powder Technology 196.2 (2009): 126-132.

45. Hapgood, Karen P. and Batool., Granulation of hydrophobic powders. Powder Technology 189.2 (2009): 253-262.

46. Rowe, R. C. Surface free energy and polarity effects in the granulation of a model system. International Journal of Pharmaceutics 53.1 (1989): 75-78.

47. He, X., et al. Development of a rapidly dispersing tablet of a poorly wettable compound—formulation DOE and mechanistic study of effect of formulation excipients on wetting of celecoxib. International Journal of Pharmaceutics 353.1 (2008): 176-186.

48. Cox, P.A., and Knox. R. B., Pollination postulates and two-dimensional pollination in hydrophilous monocotyledons. Annals of the Missouri Botanical Garden (1988): 811-818.

49. Orth, R. J., Tim JB Carruthers, Hughes et al. A global crisis for seagrass ecosystems. American Institute of Biological Sciences Bulletin 56, no. 12 (2006): 987-996.

50. Kenworthy, W. Judson, S. et al. Seagrass conservation biology: an interdisciplinary science for protection of the seagrass biome. In Seagrasses: Biology, Ecology and Conservation, pp. 595-623. Springer Netherlands, 2007.

51. Pettitt, J., Ducker, S., and Knox, B. Submarine pollination [sea grasses]. Scientific American (USA) (1981).

52. Ackerman, J.D. Sexual reproduction of seagrasses: pollination in the marine context. In Seagrasses: Biology, Ecologyand Conservation, pp. 89-109. Springer Netherlands, 2007.

53. Waycott, M., Gabriele P., Les, D.H., and Thorsten BH Reusch. Seagrass evolution, ecology and conservation: a genetic perspective. In Seagrasses: biology, ecologyand conservation, pp. 25-50. Springer Netherlands, 2007.

54. Cox, P.A. Water-pollinated plants. Scientific American-American Edition- 269 (1993): 50-50.

55. Kuo, J., and Hartog, C.D. Seagrass morphology, anatomy, and ultrastructure. In Seagrasses: Biology, Ecology and Conservation, pp. 51-87. Springer Netherlands, 2007.

56. Wetzel, R. L., and Penhale, P.A. Production ecology of seagrass communities in the lower Chesapeake Bay [Ruppia maritima, Zostera marina, Virginia]. Marine Technology Society Journal (1983).

57. Murphy, L.R., Kinsey, S.T., and Durako, M.J. Physiological effects of short-term salinity changes on Ruppia maritima. Aquatic Botany75, no. 4 (2003): 293-309.

58. Waycott, M, and Les, D.H. An integrated approach the evolutionary study of seagrasses. In Seagrass biology: proceedings of an international workshop, Rottnest Island, Western Australia, vol. 2529. 1996.

59. Arber, A. Water plants: a study of aquatic angiosperms. Cambridge University Press, 2010.

60. Laushman, R.H. Population genetics of hydrophilous angiosperms. Aquatic Botany 44, 2-3 (1993): 147-158.

61. Ducker, S. C., and Knox, R.B. Submarine pollination in seagrasses. Nature263, no. 5579 (1976): 705-706.

62. Haynes, R. R., Holm-Nielsen, L.B. and D. H. Les. Ruppiaceae. In Flowering Plants· Monocotyledons, pp. 445-448. Springer Berlin Heidelberg, 1998.

63. Mannino, M., M. Menéndez, Obrador, B., Sfriso, A., and Triest, L. The genus Ruppia L.(Ruppiaceae) in the Mediterranean region: an overview. Aquatic Botany 124 (2015): 1-9.

64. Kaul, R.B. Distribution, habitats, and taxonomy of Ruppia maritima L. and R. occidentalis S. Watson in Nebraska. (1992).

65. Sun, K., Ma, R., and Yongli Y. Studies on pollen morphology of Ruppiaceae. Journal of Northwest Normal University (Natural Science) 38, no. 1 (2001): 58-60.

66. Gifford, W.A., and Scriven, L.E. On the attraction of floating particles. Chemical Engineering Science 26, 3 (1971): 287-297.

67. Chan, D. Y. C., Henry, J.D., and White., L.R. The interaction of colloidal particles collected at fluid interfaces. Journal of Colloid and Interface Science 79, 2 (1981): 410-418.

68. Balzani, V., Credi, A., and Venturi, M. Molecular Devices and Machines Wiley. (2003).

69. Kralchevsky, P. A., Paunov, V.N., Denkov, N.D., Ivanov, I.B., and Nagayama, K. Energetical and force approaches to the capillary interactions between particles attached to a liquid-fluid interface. Journal of colloid and interface science 155, 2 (1993): 420-437.

70. Murray, C.B., Kagan, C.R., and Bawendi, M.G., Synthesis and characterization of monodisperse nanocrystals and close-packed nanocrystal assemblies. Annual Review of Materials Science 30, 1 (2000): 545-610.

71. Kralchevsky, P.A., and Nagayama, K. Capillary interactions between particles bound to interfaces, liquid films and biomembranes. Advances in colloid and interface science 85, 2 (2000): 145-192.

72. Manoharan, V.N. Colloidal spheres confined by liquid droplets: Geometry, physics, and physical chemistry. Solid state communications 139, 11 (2006): 557-561.

73. Binder, W.H. Supramolecular assembly of nanoparticles at liquid–liquid interfaces. Angewandte Chemie International Edition 44, 33 (2005): 5172-5175.

74. Davis, S. H. On the motion of a fluid-fluid interface along a solid surface. Journal of Fluid Mechanics 65, 1 (1974): 71-95.

75. Keller, J. B. Surface tension force on a partly submerged body. Physics of Fluids 10, 11 (1998): 3009-3010.

76. Kistler, S. F., and Scriven, L.E. The teapot effect: sheet-forming flows with deflection, wetting and hysteresis. Journal of Fluid Mechanics 263 (1994): 19-62.

77. Bowden, N., Choi, I.S, et al. Mesoscale self-assembly of hexagonal plates using lateral capillary forces: synthesis using the capillary bond. Journal of the American Chemical Society 121, 23 (1999): 5373-5391.

78. Grzybowski, Bartosz A., et al. Modeling of menisci and capillary forces from the millimeter to the micrometer size range. The Journal of Physical Chemistry B105, 2 (2001): 404-412.

79. Aveyard, R., and Clint., J.H. Particle wettability and line tension. Journal of the Chemical Society, Faraday Transactions 92, 1 (1996): 85-89.

80. Pieranski, P. Two-dimensional interfacial colloidal crystals. Physical Review Letters 45, 7 (1980): 569.

81. Landau, L.D., and Lifshits, E.M. Fluid mechanics, Pergamon Press, 1959.

82. Loudet, J.C., Ahmed M.A., and Yodh, A.G. Capillary interactions between anisotropic colloidal particles. Physical review letters 94, 1 (2005): 018301.

83. Menon, V. B., and Wasan, D.T. Particle—fluid interactions with application to solid-stabilized emulsions part I. The effect of asphaltene adsorption. Colloids and Surfaces 19, 1 (1986): 89-105.

84. Rapacchietta, A. V., and Neumann, A.W. Force and free-energy analyses of small particles at fluid interfaces: II. Spheres. Journal of Colloid and Interface Science 59, 3 (1977): 555-567.

85. Petkov, J.T., et al. Measurement of the drag coefficient of spherical particles attached to fluid interfaces. Journal of colloid and interface science 172, 1 (1995): 147-154.

86. Fujita, H., and Imazu, E. Motion of a Particle Floating on a Liquid Meniscus Surface. Journal of fluids engineering 114 (1992): 411.

87. Lacroix, C. R., and J.R. Kemp. 1997. Developmental morphology of the androecium and gynoecium in Ruppia maritima L.: considerations for pollination. Aquatic botany. 59: 253-262

88. Cox, P.A. 1983. Search theory, random motion, and the convergent evolution of pollen and spore morphology in aquatic plants. The American Naturalist.121: 9-31

89. Ackerman, J. D. 1995. Convergence of filiform pollen morphologies seagrasses: functional mechanisms. Evolutionary Ecology. 9:139-153

90. Richardson, F. D. 1983. Variation, adaptation and reproductive biology in ruppia maritima l. Populations from New Hampshire coastal and estuarine tidal marshes.